Clemson University

TigerPrints

All Theses   Theses

8-2008

Thermal and Structual Properties of Candidate Moldable Glass Types

Scott Gaylord
Clemson University, sgaylor@clemson.edu

Follow this and additional works at: https://tigerprints.clemson.edu/all_theses

Part of the Materials Science and Engineering Commons

Recommended Citation

THERMAL AND STRUCTURAL PROPERTIES OF CANDIDATE MOLDABLE
GLASS TYPES

A Thesis
Presented to
the Graduate School of
Clemson University

In Partial Fulfillment
of the Requirements for the Degree
Master of Science
Materials Science and Engineering

by
Scott Gaylord
December 2008

Accepted by:
Professor Kathleen Richardson, Committee Chair
Professor Ulrich Fotheringham
Professor Paul Joseph
Professor Igor Luzinov
Dr. Laeticia Petit

ABSTRACT

This thesis contains results of our efforts to develop a method for defining key glass material properties that must be known and modeled for the design and experimental validation of a precision glass molding (PGM) process for optical glasses. Viscosity, calorimetric, and thermal expansion properties of two commercial glass types N-BK7 and P-SK57 of SCHOTT were characterized to establish a proof-of-concept protocol for the experimental determination of meaningful material properties. Experimental results were determined in order to be incorporated into a computational model predicting final glass size and shape following a molding cycle. Experimental methods were confirmed on the two "known" glass types and extended to a moldable, OHARA (L-BAL35), which had never-before been characterized using this protocol, for molding applications.

Beam-bending and parallel-plate techniques were employed to measure the glass viscosity, and the well-known VFT equation was used to interpolate viscosity data through the molding region. Expansion behavior below and above the glass transition temperature, T_g and transition region was quantified using rate-heating and isothermal expansion measurements, respectively. Differential Scanning Calorimetry measurements were performed and curve-fitted using the Tool-Narayanaswamy-Moynihan (TNM) model for structural relaxation, and from these calculations kinetic glass property response in the transition region was determined. Finally, a model for predicting the thermal expansion behavior of the glass optical lens upon cooling from the molding temperature was compiled using experimentally determined variables derived within this

effort. The results show that a simple, linear thermal expansion model cannot be used and that structural relaxation must be implemented in order to precisely define the glass expansion properties upon rapid cooling through the glass transition region.

ACKNOWLEDGMENTS

I would also like to extend a "Thank You" to the entire department of MS&E, especially the hard workers in Sirrine 160 and 161 for making all the "ins and outs" possible. Their service to Clemson University, undergraduate and graduate students, and faculty is the foundation for all undertakings within all our every day needs and activities.

Of course, without the love and support from my family and my wife, Meredith Gaylord, there would be a lesser joy in all life's accomplishments. Thank you so much for being with me in all that I do.

TABLE OF CONTENTS

Page

Table of Contents (Continued)

LIST OF TABLES

LIST OF FIGURES

List of Figures (Continued)

List of Figures (Continued)

CHAPTER ONE

MOTIVATION AND RESEARCH OBJECTIVE

1.1 Motivation

Many optical systems used today are made from high quality glass optical components that are spherical in shape manufactured from conventional process of grinding and polishing. However, limitations of optical performance are being met with lens systems of spherical geometries, and it is desired to use different lens geometries (i.e. aspherical lenses) to surpass these limitations. Due to the fact that manufacturing aspherical surfaces via a grinding and polishing process is very expensive, industry has moved to a molding technique to manufacture the more optically advantageous aspherical lenses. The molding process involves heating the glass well above its glass transition temperature (T_g) to nearly its softening point temperature (viscosity of $10^{6.6}$ Pa s), where the molding takes place. The glass is held isothermally at the molding temperature for approximately a few minutes where pressing takes place before being rapidly cooled through the annealing temperature. Eventually the glass is unloaded from the mold.

The process of lens molding allows for faster and thus higher volume production. However, lens molding also induces materials engineering problems due to the fact that when the thermal history of glass is altered, its physical and optical properties such as density and refractive index, respectively, are also altered. The inherent nature of these changes comes from the structural relaxation processes: the time- and temperature-dependent change in glass properties measured in the transition region. The relaxation

behavior is unique to each and every glass composition. The optical glass made in a commercial glass manufacturing facility is carefully and slowly cooled from processing temperatures to allow long times for the relaxation of physical and optical properties. These glass properties such as density, T_g, and refractive index are reported for the glass with a specific processing condition and thermal history. If the thermal history of the optical glass is changed (i.e. in a molding application), information needs to be known with respect to the complex nature of the glass property dependence on thermal history. For example, as a lens is molded and rapidly cooled from the molding temperature, much less time is allowed for the glass to densify as compared to the large scale, bulk glass manufacturing process, which allows very slow cooling. This results in a variation from pre-molded glass properties as well as a difficulty in predicting the final shape of the lens and also a drop in the refractive index due to more free volume in a less dense glass. By studying the kinetic structural relaxation processes in the glass transition region, key issues can be resolved such as *i)* predictions of the final part geometry and thus the specific knowledge of needed mold geometries and *ii)* predictions of the final optical properties of the glass as to aid the design of the optical systems in which the molded optical component will operate.

1.2 Research Objectives

The objective of this thesis has been to develop a method of defining a process of characterizing moldable glass compositions in an effort to predict the glass behavior throughout the molding process which will define the final lens shape. The idea of

precision glass molding (PGM) optical elements is not something new, but it is a process that requires expensive and complex new-age molding machines with considerable operator experience, time, and expensive materials (both mold and glass materials). Aspects that must be overcome when molding optical elements are defining an adequate temperature profile (molding temperature) and key kinetic properties of the glass transition region that are crucial in determining the glass physical and optical property response to specific time and temperature profiles. In studying the molding process, it is the overall goal to develop key experimental processes to obtain these specific material properties that can be modeled as a function of time and temperature.

The work presented in this thesis is the result of an interdepartmental collaboration at Clemson University between the Department of Mechanical Engineering and the School of Materials Science and Engineering through a partnership with optical component manufacturers Edmund Optics and the US Army at Benét Laboratories. This team has combined expertise in materials and manufacturing to advance our understanding of the PGM process. Specifically, we have been able to combine experimental and computational efforts to predict final optical component shape and properties after molding. The Department of Mechanical Engineering carried out the modeling efforts of time, temperature and pressure parameters of the molding process. The actual manufacturing and molding equipment used for conducting the molding experiments for collaboration of process optimization is housed at Edmund Optics. Benét Laboratories supported the mold characterization capabilities, while the School of Materials Science and Engineering supported the glass and mold surface characterization abilities. The

combined expertise provided a broader knowledge in creating a scientific approach to the manufacturing of precision molded aspheric optics. Specifically, in this effort we have:

- Measured and modeled key glass properties such as glass viscosity and structural relaxation, which are required to optimize the time, temperature, and pressure profiles of the molding process and lead to knowledge of the final physical and optical glass properties.

- Implemented the key glass property parameters into a working mechanical model that helped predict the final lens shape and thus helped identify the specific mold design needed to achieve such geometries within tight tolerances.

Within the School of Materials Science and Engineering, the focus of the glass characterization project – the focus of the bulk of this thesis – was on the development of an experimental method that determined the important kinetic material properties defining post heating and cooling structural relaxation. By defining these compositional dependent structural relaxation properties, a working model of the molding process can be used eliminating a "trial and error" production method. The development of our methods at Clemson University have been used to validate previous conclusions made for commercial SCHOTT optical glasses BK-7 (presumed to be similar in composition to N-BK7) and P-SK57, and then applied to L-BAL35 (of OHARA) as an optical glass that has been characterized for molding applications. Moreover, as there are more than 30 glass types from various glass companies that have been recently developed for precision molding, it was the goal of this thesis to define a method that can be applied to any new glass type that is desired to be precision molded. The specific questions addressed

through the work of this thesis pertaining to the characterization of glass viscosity and structural relaxation properties are:

1. What is the glass viscosity response to temperature and how do we measure it repeatably?

2. How do we accurately measure the specific heat, c_p, and thermal expansion coefficient, α, characteristics of the investigated glasses?

3. How can we model the kinetic c_p and α behavior through the glass transition region so that specific glass properties can be implemented into a mathematical model predicting the affect of the molding cycle (more specifically the cooling profile) on the final lens size and shape?

The results of efforts to address these questions are contained in this thesis.

CHAPTER TWO

INTRODUCTION

Typical, conventional processes for manufacturing optics involve a grinding and polishing technique that has been perfected throughout the years for producing high volume spherical shaped optics. However, spherical optics can be plagued with imaging errors such as spherical aberration requiring additional corrective optical components leading to the assembly of bulkier systems. The alternative is to manufacture lenses with aspherical surfaces that do not induce the imaging errors that require additional components to correct. Such lenses are very advantageous for applications in cameras, sensors, and detectors that supply entertainment, medical, and military and homeland security industries alike. The demands for higher quality and more efficient optical systems in these industries require the investigation of methods for manufacturing aspherical surfaces via methods other than slow speed and low volume grinding and polishing techniques. While some of these newly developed techniques for fabricating aspherical geometries are sophisticated methods of grinding and polishing, such as magnetorheological finishing, they are slow and remain extremely costly.

While grinding and polishing of aspherical surfaces can be done, the idea of molding glass lenses has been introduced and studied for some time now as a method to develop higher volume production of glass optical lenses [1-3]. The process involves heating a glass beyond the transition region and into the liquidous region, where pressing for some specified amount of time takes place. This temperature where molding takes place has

been shown and described to be at temperatures above T_g and at temperatures where the glass begins to deform under its own weight (otherwise known as the dilatometric softening point, T_s) but below the Littleton softening point temperature. The T_s is understood to correspond to a viscosity of approximately $10^{8.0}$ Pa s [4], and the Littleton softening point temperature corresponds to a viscosity of $10^{6.6}$ Pa s [5]. Studies have shown results for molded BK-7 and SF-6 with published viscosity and molding temperature information indicating that an appropriate molding temperature was at approximately a viscosity of $10^{8.0} - 10^{6.6}$ Pa s [6-9].

After pressing from the molding temperature, the lens is cooled to temperatures below the transition region of the glass at which point the thermal shrinkage of the lens is strongly dependent upon the cooling rate as depicted in Fig. 2.1 below.
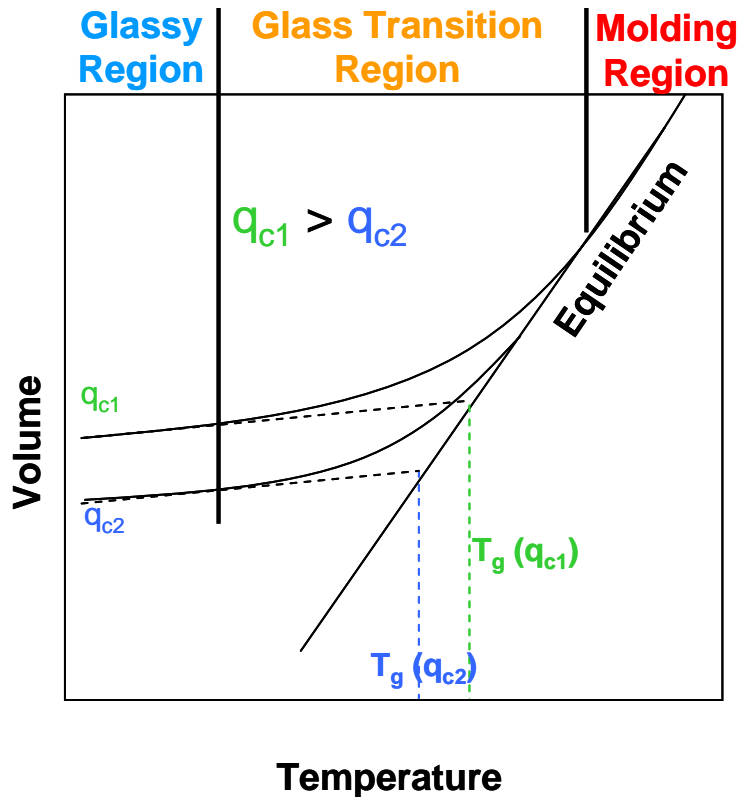
Fig. 2.1: Schematic depicting the glass volume shrinkage as a function of temperature when cooled from the molding temperature through the glass transition region at different cooing rates q_{c1} and q_{c2}.

As the glass cools from the equilibrium liquid in the molding region to temperatures below the GLASS TRANSITION region, the intersection of the equilibrium liquid and the "glassy" volume-temperature line is commonly referred to as the glass transition temperature, T_g [10]. The T_g shown in Fig. 2.1 above can also be referred to as the fictive temperature, T_f, which is the temperature at which the glass structure would be at equilibrium [11] – the subject and concept of the T_f will be discussed further in section 2.2. At a faster cooling rate q_{c1}, the T_g is indicated to be higher and the volume shrinkage less than what occurs for a slower cooling rate q_{c2}. A faster cooled glass is less dense than a slow-cooled glass. If a simple thermal expansion model only incorporating the

change in volume with a change in temperature and neglecting a kinetic (time) response is modeled, then the lens shape deviation from the mold geometry cannot be accurately predicted [6, 8]. The cooling rate dependence of the glass shrinkage leading to a deviation of lens shape from the mold shape must be defined with a structural relaxation model that predicts the time and temperature dependence of glass volume changes in the transition region [7, 12, 13]. The incorporation of material parameters defining the kinetics of the glass transition region provide a more realistic thermal expansion model agreeing with what is described within the schematic in Fig. 2.1 than one that is simply defined by a single thermal expansion coefficient. Therefore, not only does the viscosity-temperature behavior of the glass greatly dictate processing conditions, but also the time and temperature dependent glass volume response is crucial for predicting the final molded lens shape [7].

2.1 Glass Viscosity

The viscosity of glass at high temperatures is a measure of the resistance to flow of the fluid melt. The temperature dependence of the glass viscosity in the limited range of temperatures in the glass transition region is typically defined with an Arrhenius expression [4, 10]

$$\eta = \eta_0 e^{\frac{E_\eta}{RT}} \, ,$$ (2.1)

where η is the viscosity (Pa s), η_0 is a constant, E_η is the activation energy for viscous flow, R is the ideal gas constant (kJ mol^{-1} K^{-1}), and T is the temperature (K). However, at higher temperatures where the glass melt is much less viscous, the E_η value is less as

would be expected. For this reason, a better fit to the entire temperature range is typically used, which was studied by Fulcher and is referred to as the Vogel-Fulcher-Tamman (VFT) equation seen below [14]

$$Log\,\eta = A + \frac{B}{T - T_0},$$ (2.2)

where A, B, and T_0 are constants, and T is temperature (^{o}C).

A generalization about the viscosity behavior as a function of temperature has been studied to classify glass compositions as 'strong' or 'fragile' [15]. The categorization of glass viscosity behavior by a high fragility parameter, m, refers to a glass with a *floppy* network—defined as a network where the number of constraints is less than the number of degrees of freedom—is expected to exhibit a viscosity which is highly dependent on the temperature. A strong glass with low m has a more *rigid* network—described as an over constrained network—and has a viscosity with less prevalent temperature dependence. The degree to which a glass melt is considered strong or fragile can be quantified by normalizing the E_η value with respect to the temperature at the viscosity of $10^{12.0}$ Pa s, $T_{12.0}$ – which is commonly associated with the glass transition [15] – by applying the following equation [16, 17]

$$m \cong \frac{E_\eta}{RT_{12.0}Ln(10)}.$$ (2.3)

Seen below in Fig. 2.2 is a viscosity-temperature curve with some of these key characteristic features.
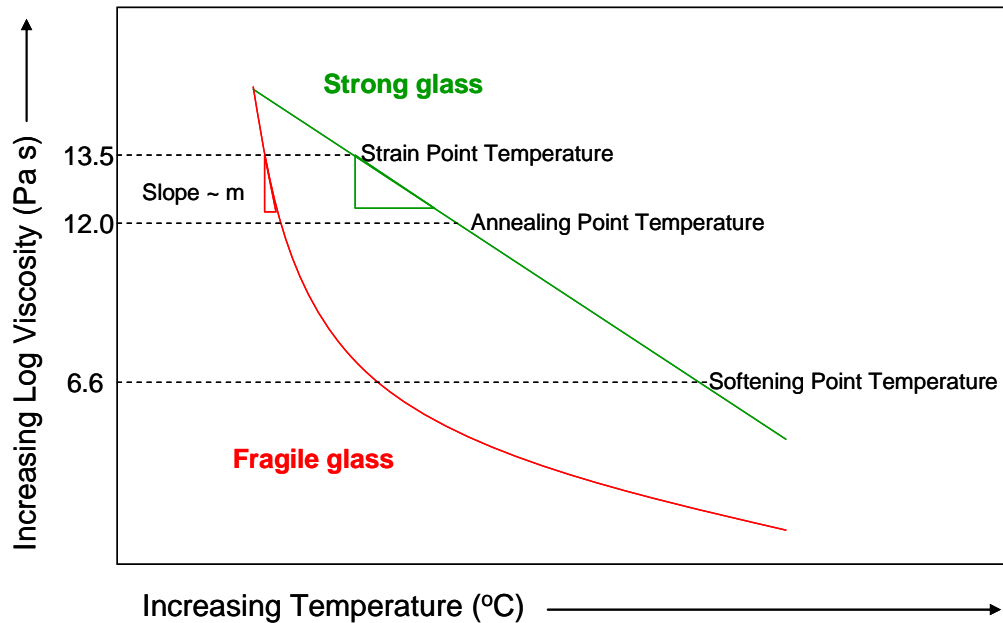
Fig. 2.2: Viscosity-temperature curve with the fragility parameter, m, strain, annealing, and softening point indications.

Fig. 2.2 shows the rather linear temperature dependence of the Log viscosity near the $T_{12.0}$ for both fragile and strong glasses quantified by m, and it is reasonable to see how an Arrhenius relationship according to equation (2.1) could be applied in this region. However, for higher temperatures and fragile glasses, it is shown how a modified viscosity-temperature equation is needed such as the VFT formulation shown in equation (2.2). Also, three key viscosity-temperature points are shown: the strain, annealing and softening point temperatures, where Log viscosities of 13.5, 12.0, and 6.6 Pa s are represented respectively [18-20].

For viscosity determination in the annealing range of glass (approximately in the viscosity range between Log 13.0 and Log 11.0 Pa s), the beam-bending technique was established as an efficient and precise method of measuring the viscosity of glass beams

11

in constant temperature or rate-heating modes [21]. It has been used by several authors to measure the viscous response of inorganic oxide [21] and metallic glasses alike [22-24]. It was shown by Busch *et al* in [22] that the glass viscosity in the annealing region changes in an apparent exponential fashion with time during an isothermal test. This confirmed discussions by Scherer [10] that the glass density changes slowly at temperatures in the annealing range until it reaches its equilibrium value, and the viscosity is expected to follow inversely with free-volume. In actuality, the changing viscosity (changing density) does not change precisely exponentially due to a combination of non-linear and non-exponential effects, and the details of this behavior will be discussed in section 2.2 and 2.3.

In the lower viscosity regime of the softening range, the parallel plate viscometer has been used for viscosity measurements of glass, solid right-cylinder disks pressed between two parallel steel plates [25]. Original development of the theory and application of the parallel plate viscometer was studied for viscosity measurements of polyethylene and vinyl chloride-acetate [26] and coal-tar pitch [27]. Unlike the beam-bending technique, measurements in the softening range are typically well above the Glass transition region and therefore the kinetics of glass response is instantaneous. This allows instrument testing to be performed at a 5 K min^{-1} heating rate providing large amounts of data points at a wide range of temperatures [25].

To experimentally measure the viscosity in both the annealing and softening regions, American Society for Testing and Materials (ASTM) standards C598-93, CM1350 M-96 and C1351 M-96 are used [18-20]. A SCHOTT glass P-SF67 was used as a reference

material for ASTM C598-93 and CM1350 M-96 standard tests as viscosity information was known through private communication [28].   NIST 710a glass was used as a reference material for ASTM C1351 M-96 standard tests as its viscosity data is published by NIST.

2.2 Structural Relaxation

While the glass viscosity behavior gives information of molding temperatures, studies of glass structural relaxation give insight into the time and temperature dependent path of changing glass properties – most specifically, glass volume [10]. This gives an indication of how the volume changes when being rapidly cooled through the transition region immediately after molding. The figure below gives a simplified depiction of structural relaxation as it pertains to the relationship between glass volume, temperature, and time in the transition region for a glass formed via different cooling rates (q_{c1} and q_{c2}).
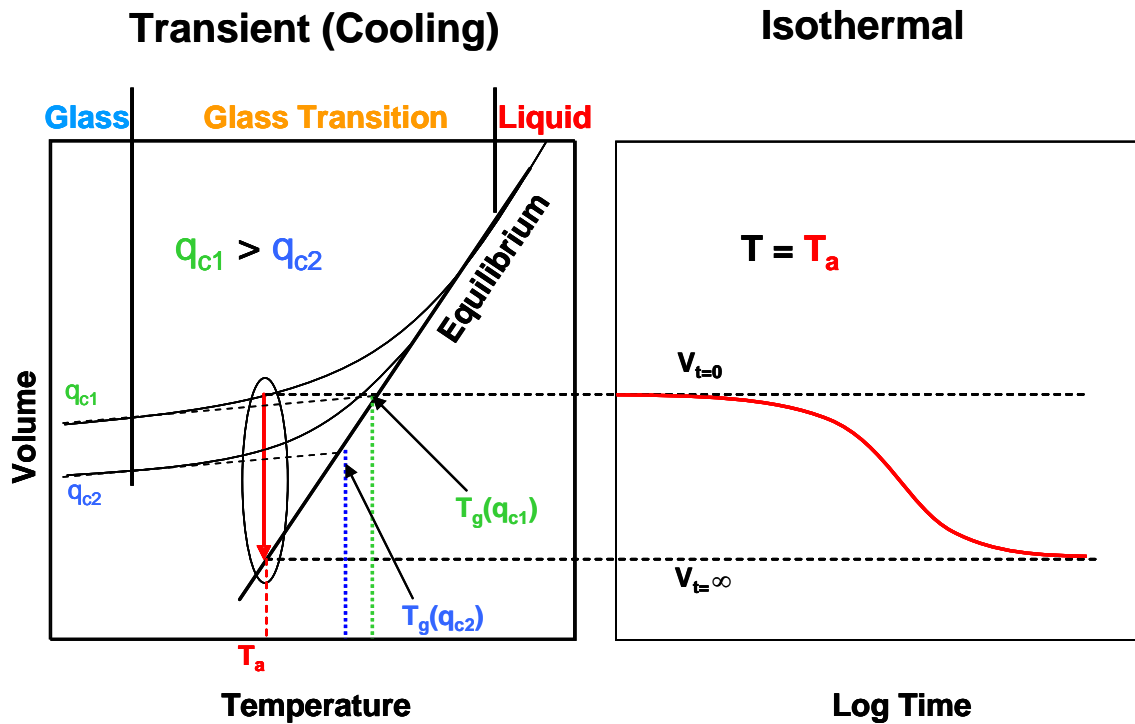
Fig. 2.3: Schematic depicting glass structural relaxation of volume in the glass transition region.

As seen in the transient case in Fig. 2.3 (left), as the glass is cooled at some rate from the liquid state, it enters the glass transition region and the volume begins to deviate from its equilibrium state. As one might imagine, the glass structural state also deviates from equilibrium when being cooled into the transition region. After cooling below the transition region, the obtained limiting structural state of the glass is defined in terms of the liming value of the fictive temperature, T_f, which coincides with the T_g found by the intersection of the "glassy" and "liquid" lines shown in Fig. 2.3 (and also Fig. 2.1). Therefore, the T_f is defined as the temperature at which the glass structure would be at equilibrium and was first defined and introduced by Tool [11]. Similar to the description of T_g above, T_f responds in the same way with respect to cooling rate, as a higher T_f

results from a higher cooling rate rather than a lower cooling rate from the liquid state. Furthermore, a glass cooled into the transition region, and then suddenly held at an isothermal temperature, T_a, results in a time-dependent relaxation of the glass' volume towards its equilibrium state, and similarly a relaxation of T_f toward T_a.

The unique characteristics of the change in glass dimension (whether one- or three-dimension) with respect to temperature through the Glass transition region can be explained in terms of the changing equilibrium structure of the glass, or T_f. Tool originally investigated this phenomenon providing the definition for the fictive temperature and directly quantifying it with respect to thermal expansion measurements [11]. Tool's original idea described the change in T_f with respect to change in T $\left(\dfrac{dT_f}{dT}\right)$ by quantifying the linear dilatometric response of glassy systems. The representation of his model with respect to volume (the same equations apply for the linear response) is shown below in the following way

$$\frac{dT_f}{dT} = \frac{\alpha_V(T) - \alpha_{V,g}}{\alpha_{V,l} - \alpha_{V,g}} = \alpha_N ,$$ (2.4a)

$$\Rightarrow \frac{dV}{V_0} = \left(\alpha_{V,l} - \alpha_{V,g}\right)dT_f + \left(\alpha_{V,g}\right)dT ,$$ (2.4b)

where $\alpha_V(T)$ is the apparent volume thermal expansion coefficient through the entire range of temperature defined by $\alpha(T) = \dfrac{dV}{V_0 dT}$, $\alpha_{V,g}$ is the "glassy" volume thermal expansion coefficient (taken by the slope of the volume-temperature expansion line in Fig. 2.3 below the Glass transition region) and $\alpha_{V,l}$ is the "liquid" volume thermal expansion

coefficient (taken by the slope of the volume-temperature expansion line in Fig. 2.3 above the Glass transition region). Equation (2.4a) is also referred to as the normalized thermal expansion coefficient, α_N. The equation (2.4b) is derived from (2.4a) where the equation for the change in volume normalized to the original volume $\left(\dfrac{dV}{V_0} \right)$ is given.

Malek *et al* performed not only rate-heating and cooling, but also isothermal dilatometric experiments in the glass transition region of As_2S_3 [29] and As_2Se_3 [30] glass networks. By performing isothermal experiments in the Glass transition region, the T_f of the glass could be monitored by making short temperature-jumps after an equilibration period and measuring the expansion or contraction as a function of time. Direct determination of the relaxation kinetics was found from these isothermal experiments. The results were successfully applied to model rate-heating expansion data. Furthermore, in this way, the dT_f and dT could be controlled (and be made equivalent after long times), which yielded fairly accurate data quantifying the α_l (equation (2.4a)) (note here that the term α refers to the *linear* expansion coefficient, which is typically used to discuss expansion properties as is in [29-32] and is so throughout the remainder of this document). Fotheringham *et al* preferred to perform similar annealing experiments, but rather than measure the expansion or contraction in real time at the test temperature in a dilatometer as was performed by Malek *et al* [29, 30], the samples were quenched to room temperature for length measurements, and data points were generated at intervals of approximately 5 – 10 hours [31, 32]. However, Fotheringham *et al* did not use this method to quantify the relaxation kinetics or the α_l, but rather to confirm the

determined relaxation kinetics from rate-heating analyses. More recently, precise methods have been developed to measure the α_l of glass with a dilatometer, by testing cylindrical glass samples contained inside a cylindrical metal sample holder, which eliminates any sample deformation that can result from the nominal force of the sample probe [33].

As one might imagine, for changes in the volume properties of a glass, there are also similar changes in the enthalpy – quantified by precise specific heat, c_p, measurements. It has been shown for B_2O_3 glass that the relaxation of the enthalpy and refractive index were different, indicating that there may not be a universal equilibrium temperature value for all properties such as enthalpy and volume [34]. However, several authors have shown for a variety of inorganic glasses (borosilicates, soda-lime-silicates, and chalcogenide) and polymers that the kinetics defining the structural relaxation of volume are experimentally indistinguishable from that of enthalpy [31-33, 35, 36]. In fact, the $\left(\dfrac{dT_f}{dT}\right)$ for glassy materials has been characterized in the same way as described in equation (2.4a), but with respect to the c_p as shown below

$$\frac{dT_f}{dT} = \frac{c_p(T) - c_{p,g}}{c_{p,l} - c_{p,g}} = c_{p,N},$$
(2.5)

where now, $c_p(T)$ is the apparent specific heat through the entire range of temperature, $c_{p,g}$ is the c_p in the glassy state, and $c_{p,l}$ is the c_p in the liquid state. The equation (2.5) is also referred to as the normalized specific heat, $c_{p,N}$.

The use of the equation (2.5) has been used to analyze c_p data by integrating the c_p across the entire glass transition region according to

$$\int_{T^*}^{T_{f,0}} \left(c_{p,l} - c_{p,g} \right) dT_f = \int_{T^*}^{T'} \left(c_p(T) - c_{p,g} \right) dT ,$$

(2.6)

where T* is an upper-bound temperature just above the Glass transition region corresponding to a $c_{p,l}$ value, T' is a temperature well below the Glass transition region corresponding to a $c_{p,g}$ value, and $c_p(T)$ corresponds to all c_p values between $c_{p,g}$ and $c_{p,l}$ [34, 37, 38]. In this way, the T_f can be computed as a function of temperature through the transition region, and the limiting fictive temperature value or initial fictive temperature value of the glass, $T_{f,0}$, can be determined.

2.3 Numerical Simulation of the Tool-Narayanaswamy-Moynihan (TNM) Model

The original model describing the time and temperature-dependent path of the fictive temperature relaxation was postulated by Tool who proposed the following differential equation [11]

$$\frac{dT_f(t)}{dt} = \frac{T(t) - T_f(t)}{\tau} ,$$

(2.7)

where t is time, T temperature, and τ the relaxation time. The temperature dependence of the relaxation time was originally explained with the following Arrhenius relationship

$$\tau = \tau_0 e^{\frac{E}{RT}} ,$$

(2.8)

where τ_0 is the relaxation time constant, E the activation energy, and R the ideal gas constant. In an isothermal case, where a glass sample has an initial fictive temperature

18

$T_f(0)$ and is exposed to a temperature, T, the solution to equation (2.7) describes the relaxation of the T_f in the following way (for derivation see **Appendix A**)

$$T_f(t) = T + \left(T_{f,0} - T\right) \cdot e^{\frac{-t}{\tau}} . \tag{2.9}$$

However, the above postulated model could not adequately predict Tool's experimental data, and the reason may be due to the lack of T_f dependence of the relaxation time, τ. Equation (2.7) was modified by Narayanaswamy changing the simple Arrhenius equation by introduction a degree of non-linearity quantified by the parameter x that ranges between 0 and 1 shown in the following equation [39].

$$\tau = \tau_0 \cdot e^{\left(\frac{E}{R}\left(\frac{x}{T} + \frac{1-x}{T_f}\right)\right)} . \tag{2.10}$$

By stating the T_f dependence of τ and introducing the non-linearity parameter x, one finds a faster relaxation time when T_f is greater than T and a slower relaxation time when T_f is less than T. This means that the relaxation time depends not only on the magnitude of the difference between T_f and T but also the direction of that difference [40, 41]. The derived Tool-Narayanaswamy (TN) model can be seen by inserting equation (2.9) into equation (2.6)

$$\frac{dT_f(t)}{dt} = \frac{T(t) - T_f(t)}{\tau_0 \cdot e^{\left(\frac{E}{R}\left(\frac{x}{T} + \frac{1-x}{T_f}\right)\right)}} . \tag{2.11}$$

An additional comment of the above derivation of the TN model was discussed by Narayanaswamy [39] with respect to the use of equation (2.7) in that a single exponential relaxation function was not found to be sufficient in describing the thermal history of the

glass. In fact, by the incorporation of the non-exponentiality factor, β, the further

contributions to the TN model by Moynihan [37] further defined an approximation of the

isothermal case to be described in the following way

$$T_f(t) = T + (T_f(0) - T) \cdot e^{\left(-\left(\frac{t}{\tau}\right)^{\beta}\right)}, \tag{2.12}$$

where β ranges in value from 0 to 1. In addition to the incorporation of the β parameter,

equation (2.12) differs from equation (2.9) in that the relaxation time in equation (2.12)

depends on both temperature and fictive temperature according to equation (2.10). For

this reason, equation (2.12) can only be used as an approximation for an isothermal case

and only when $T_f(0)$ is close to T. To revert back to the form of the more simple

exponential relaxation function in terms of a Prony series, the following conversion to

sum n number of simple exponential functions can be made and is given by

$$e^{\left(-\left(\frac{t}{\tau}\right)^{\beta}\right)} = \sum_{i=1}^{n} \upsilon_i \cdot e^{\left(\frac{-t}{\tau_i}\right)} \text{ and } \sum_{i=1}^{n} \upsilon_i = 1, \tag{2.13}$$

where τ is as defined in equation (2.10) above, and τ_i is defined as

$$\tau_i = \tau_{0,i} \cdot e^{\left(\frac{E}{R}\left(\frac{x}{T} + \frac{1-x}{T_f}\right)\right)}. \tag{2.14}$$

In this way, some τ_i values are smaller than τ, which model experimental cases of the fast

kinetics of relaxation function at small time, and some τ_i values are larger than τ

explaining the slow kinetics of the relaxation at large time [31, 42]. With the

introduction of multiple relaxation times τ_i, is reasonable to see that there are multiple T_f

values such that each τ_i is responsible for the relaxation of separate fictive "sub" temperatures $T_{f,i}$, weighted with υ_i [37]

$$T_f = \sum_{i=1}^{n} \upsilon_i \cdot T_{f,i} \ . \tag{2.15}$$

As one might imagine, each the individual differential equation for each $T_{f,i}$ with respect to time is as follows

$$\frac{dT_{f,i}}{dt} = \frac{T(t) - T_{f,i}(t)}{\tau_i} , \tag{2.16}$$

where τ_i is defined as shown in equation (2.14). With these contributions from Tool, Narayanaswamy, and Moynihan, the well-known (TNM) model results in the following differential equation describing the change in T_f with respect to change in time as

$$\frac{dT_f}{dt} = \sum_{i=1}^{n} \upsilon_i \cdot \frac{T - T_{f,i}}{\tau_{0,i} \cdot e^{\left(\frac{E}{R}\left(\frac{x}{T} + \frac{1-x}{T_f}\right)\right)}} , \tag{2.16}$$

or with respect to temperature

$$\frac{dT_f}{dT} = \frac{1}{\dot{T}} \sum_{i=1}^{n} \upsilon_i \cdot \frac{T - T_{f,i}}{\tau_{0,i} \cdot e^{\left(\frac{E}{R}\left(\frac{x}{T} + \frac{1-x}{T_f}\right)\right)}} , \tag{2.17}$$

where $\dot{T}$ is the linear rate of heating or cooling $\left(\frac{dT}{dt}\right)$.

From the resulting TNM model, the four material parameters that define the kinetics of the glass transition region are E/R, x, β, and τ_0. These four values have been determined from c_p measurements modeled with the above set of differential equations of the TNM model, and the values have been compiled for over 30 inorganic (oxide and

non-oxide) and organic (polymers) glassy systems alike [43]. Some of these values and

others defined in optical glasses and some polymers are shown below in Table 2.1.

Table 2.1:   Structural relaxation parameters of the TNM model for different glassy
materials compiled from different authors.

	E/R (K)	x	β	τ_0 (s)	Ref.
BK-7*	71,802.3	0.695	0.694	8.75×10^{-36}	[32]
P-SK57*[†]	84,396.5	0.789	0.656	1.68×10^{-46}	[44]
P-LaSF47*[†]	103,154	0.899	0.524	5.76×10^{-54}	[44]
B_2O_3	45,249	0.40	0.65	1.51×10^{-33}	[34]
As_2Se_3	41,126	0.49	0.67	7.6×10^{-38}	[38]
As_2Se_3	38,300	0.57	0.71	3.98×10^{-35}	[30]
As_2S_3	32,355	0.31	0.82	1.07×10^{-27}	[29]
Polystyrene	80,000	0.49	0.74	1.89×10^{-92}	[45]
a-PMMA	138,000	0.19	0.35	4.07×10^{-156}	[45]
Polycarbonate	150,000	0.19	0.46	3.01×10^{-155}	[45]

*Commercial glass types of SCHOTT.   [†]Commercially developed moldable glass types.

The table above shows the large variation of the structural relaxation parameters between

different systems, which exhibit a glass transition, determined by various authors. The

different compositions shown in Table 2.1 indicate that the inorganic, non-oxide glasses

and the polymers have structural relaxation behavior that is distinctly different from one

another noted specifically by the extreme E/R and τ_0 values. Likewise, the commercial

oxide glasses have structural relaxation parameters that are mid-range between those of

polymers and inorganic, non-oxide glasses. Also shown in Table 2.1 are two glasses P-

SK57 and P-LaSF47, commercially developed for precision molding (hence the "P"

description). Fotheringham *et al* studied the structural relaxation processes of these glass

types in efforts to predict how the refractive index changes as a function of cooling rate [44].

It is our goal within this effort to bring the capability of viscosity and structural relaxation characterization to Clemson University so that it can be directly imported into a working, self-sufficient finite element model for predicting glass lens shape throughout a precision molding process. Optical glasses N-BK7 (SCHOTT), P-SK57 (SCHOTT), and L-BAL35 (OHARA) were chosen as glasses to be characterized for rheological and structural relaxation attributes for applications to a molding process. N-BK7 is an optical glass with the same optical properties as the borosilicate BK-7. However, N-BK7 is a "green" glass (denoted by the "N" description), which means that environmentally unacceptable fining agents such as arsenic have been removed. P-SK57 glass is a silicate glass whose position on the Abbe diagram (n_d = 1.58700 and v_d = 59.60) is similar to that of L-BAL35 (n_d = 1.58913 and v_d = 61.15) indicating that they may be similar in glass composition. As information has been previously researched and reported for BK-7 and P-SK57 glass types with respect to structural relaxation and BK-7 and N-BK7 glasses are presumed to be similar in composition, these glasses were first characterized to develop experimental capabilities and validate measurement techniques. The realized procedures from studying these two glass types were then applied to a previously unstudied glass type – the moldable L-BAL35 of OHARA. The experimentally determined quantities resulting from our measurements were used in a computational model being developed in the Department of Mechanical Engineering at Clemson University. Subsequently, predictions of material response from the model were compared to actual molding results

compiled on L-BAL35 on the Toshiba molding machine at Edmund Optics, Pennsburg, PA.

CHAPTER 3

EXPERIMENTAL METHODS

The experimental methods developed within the present study were to establish the capability here at Clemson University to define the key properties of optical glass that can be used to model lens shape through a molding process. The results of the material characterization data and its use in our model lead to final size and shape predictions. Furthermore, the work within this thesis establishes the foundation for a model capable of optical glass property changes (i.e. refractive index) inherently induced by the lens molding process.

Rheological and expansion properties of glass materials were measured to understand the key characteristics that define the molding conditions and the ultimate optical performance. More specifically, N-BK7 (SCHOTT), P-SK57 (SCHOTT), L-BAL35 (OHARA) and glass types were characterized for their temperature-viscosity response in the lens molding region. Thermal expansion coefficient and specific heat properties were measured as a function of time, temperature, and glass composition. The Tool-Narayanaswamy-Moynihan (TNM) model of the kinetics of the glass transition region was applied to experimental specific heat and expansion data to define the specific TNM model parameters. These parameters were then used to define and predict time and temperature dependent glass properties in the glass transition region.

3.1 Glass Viscosity Instrumentation and Characterization

3.1.1 Instrumentation

The glass viscosity properties in the annealing range (Log 11.0 – Log 13.0 Pa s) were measured via a BBV-1000 beam bending viscometer of Orton Ceramics [46]. The instrument components can be seen in the Fig. 3.1 below.
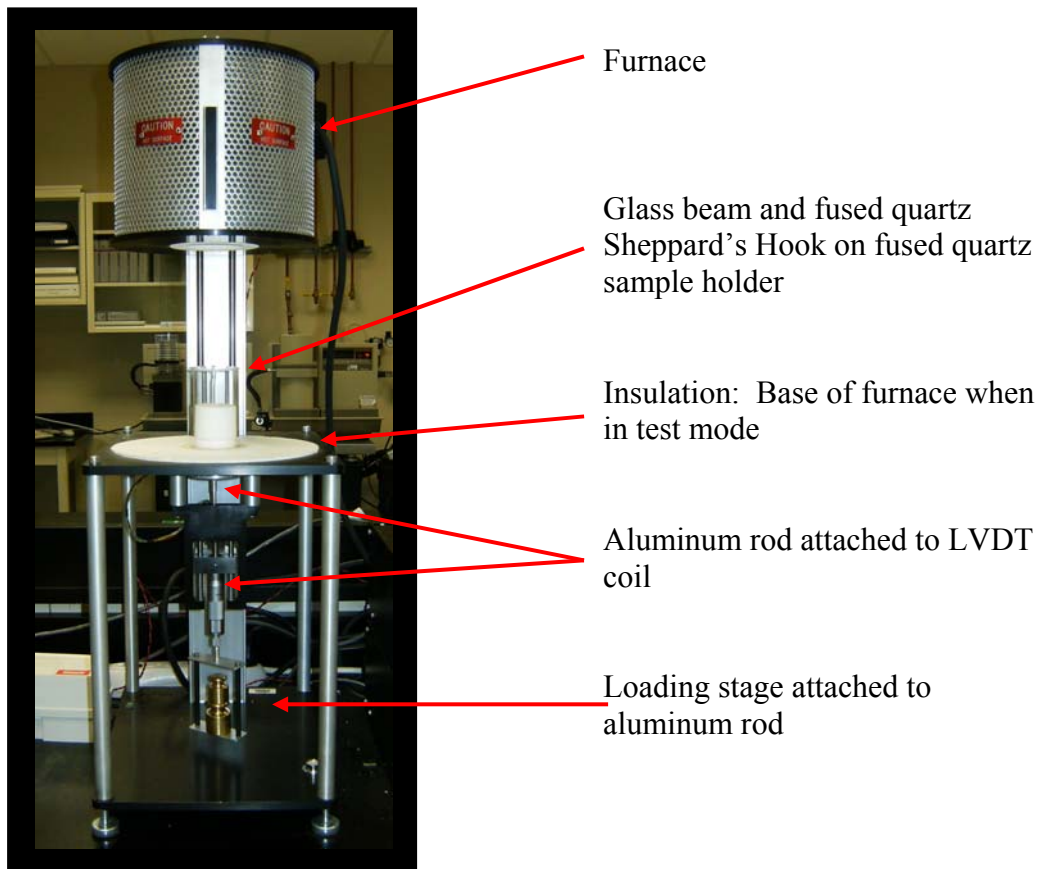
Fig. 3.1: BBV-1000 beam-bending viscometer, Orton Ceramics [46].

The BBV has a furnace capable of reaching 1000°C, equipped with a type "S" controller and sample thermocouple, and constructed with a diameter of 65 mm, which easily slides over the glass sample mounted on the fused quartz sample holder (Fig. 3.2).

Glass Sample

Fused quartz sample holder

Fused quartz "Sheppard's hook"

Insulation around sample holder

Insulation at base of furnace when in test mode
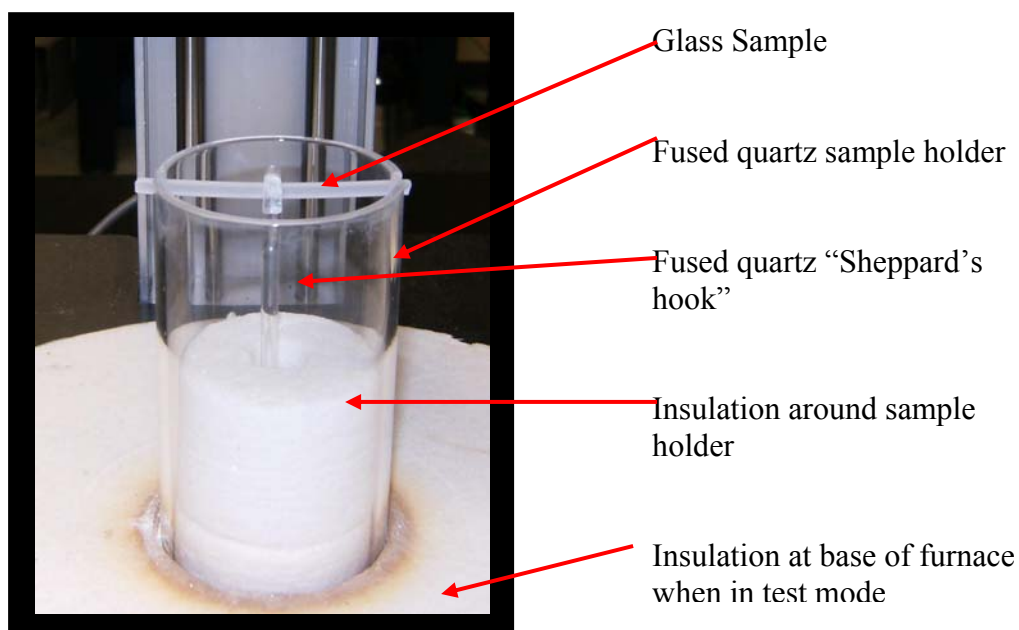
Fig. 3.2: BBV-1000 experimental set-up with glass sample beam mounted on the fused quartz sample holder with the fused quartz "Sheppard's hook" applied at the midpoint of the sample.

The 50 mm diameter fused quartz sample holder supports a glass beam with square, rectangular, circular, or elliptical cross-section that must have dimensions maintaining a cross-sectional moment of inertia between 2×10^{-4} and 10×10^{-4} cm^4[18]. At the midpoint of the glass sample is a fused quartz "Sheppard's hook", which is attached to an LVDT coil beneath the furnace. At the base of the LVDT coil is attached an aluminum load-bearing stage, where weights are applied. The LVDT monitors the deflection rate of the glass sample as a function of temperature (for rate-cooling or rate-heating measurements) or time (for isothermal measurements).

The glass viscosity properties in the softening region (in the range of Log 4.0 – Log 8.0 Pa s) of the glass were measured with a PPV-1000 parallel-plate viscometer of Orton Ceramics [47]. The instrument components are seen in the Fig.3.3 below.
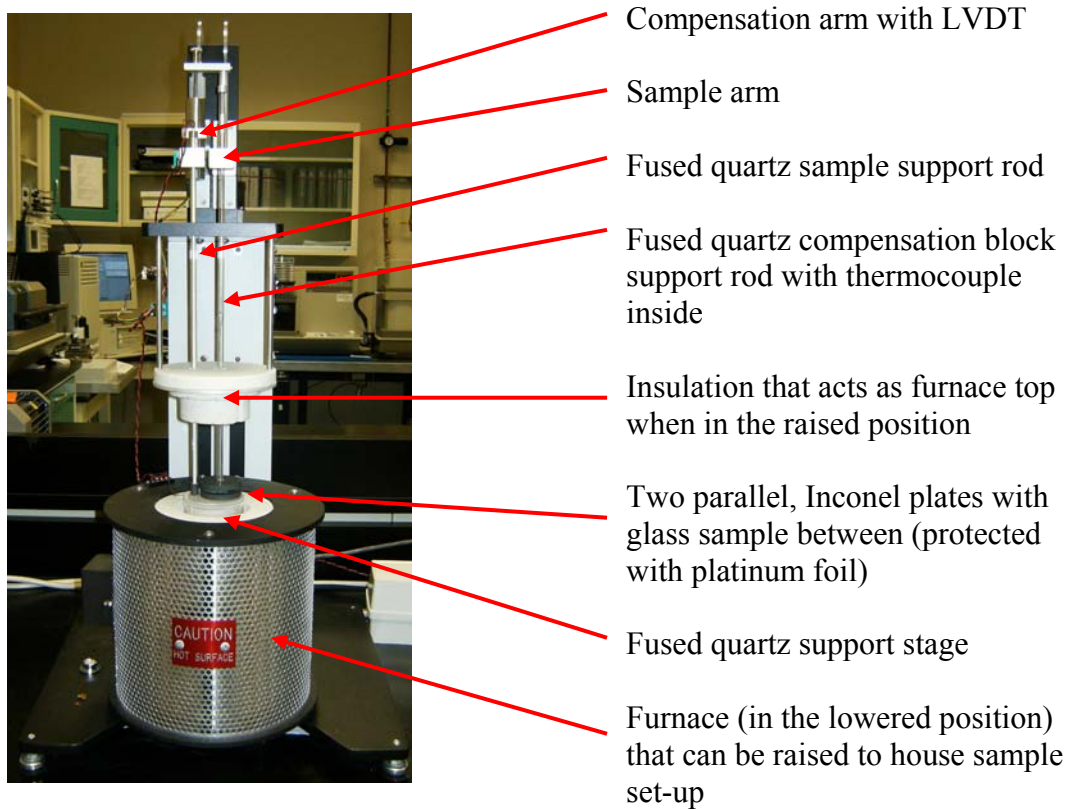
Fig. 3.3: PPV-1000 parallel plate viscometer, Orton Ceramics [47].

At the top of the instrument is the sample arm that is attached to the experimental set-up inside the furnace with a fused quartz support rod. As the sample height changes as a function of time and temperature, an LVDT coil – residing on the compensation arm and attached to the adjacent sample arm – monitors the magnitude and direction of the height change. The compensation arm is attached via a hollow, fused quartz support rod to the inconel compensation block (12 mm thickness), which houses the sample temperature thermocouple that rests on top of the inconel compensation block (the type "S" sample thermocouple resides 35 mm from the glass sample). By attaching the LVDT to the inconel compensation block, system movement and inconel plate expansion are nullified

from the LVDT signal. The insulation (seen above the sample experimental set-up) acts as the top of the furnace in the raised position for experimental measurements. The 1000°C Kanthal wound, ceramic fiber lined furnace (with type "S" control thermocouple) can be raised and lowered with a motor to house the glass sample seen in the Fig. 3.4 below.

Fused quartz support rod with thermocouple inside resting on compensation block

Fused quartz sample support rod

Parallel inconel plates protected with platinum foil

Glass sample

Fused quartz support stage
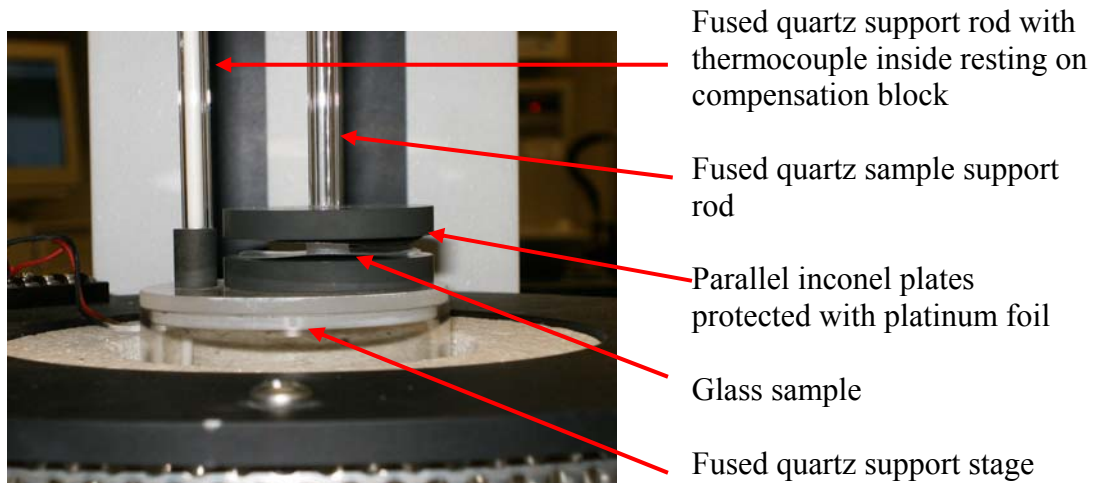
Fig. 3.4: PPV-1000 experimental set-up with glass sample disk between parallel, inconel plates.

The solid right cylinder glass sample 3 – 6 mm in height and 6 – 12 mm in diameter (faces fine ground finish) resides between two parallel, inconel plates lined with platinum foil (0.0254 mm thick), which is supported atop a fused quartz stage. The top inconel plate is attached to the fused quartz sample support rod. The application of the load to the glass sample is done by attaching weights to the sample arm at the top of the instrument. The LVDT monitors the deflection rate of the glass sample as a function of temperature (for rate-cooling or rate-heating measurements) or time (for isothermal measurements).

3.1.2 Experimental method

Isothermal viscosity measurements of the investigated glasses in the annealing range (Log 11 – Log 13 Pa s) were measured of glass rectangular beams (about 3 x 3 x 55 mm) prepared with fine-ground faces. The glass sample was loaded onto the fused quartz sample holder at room temperature. The furnace was then increased to the test temperature in the annealing range of the glass, which was chosen to be different from the industry reported annealing point temperature of the glass, $T_{12.0}$, reported by the glass manufacturer by no more than 15°C ($T_{BBV} = T_{12.0} \pm 15^{o}$C). Temperature stabilization was assumed when the furnace maintained the target test temperature for three minutes. Then a load of 200 – 400 g was applied to the midpoint of the beam by a fused quartz "Sheppard's hook" that passed through an LVDT. After temperature stabilization and application of the load, the midpoint deflection (h) was monitored as a function of time until the deflection rate became constant. The viscosity was calculated according to the following equation [19].

$$\eta = \frac{gL^3}{1440 I_c \left(\dfrac{dh}{dt}\right)} \left(M + \frac{\rho AL}{1.6}\right) \tag{3.1}$$

,

where η is the viscosity (Pa s), M the applied load (g), dh/dt the midpoint deflection rate of test beam (cm/s), g the acceleration of gravity (980 cm/s^2), I_c the cross-sectional moment of inertia (cm^4), ρ the density of glass, (g/cm^3), A the cross-sectional area of the beam (cm^2), and L the support span (cm).

Experimental errors of the beam bending measurements can be attributed to the confidence of the Type "S" thermocouple, which is approximately $\pm 1^{o}$C, and the

neglected thermal expansion of the sample and fused quartz stage. However P-SF67 glass of Schott was used as a standard with a published viscosity of Log 12.0 Pa s at 546°C [48] to correct for any accrued experimental error.

Rate-heating viscosity measurements of the investigated glasses in the softening range (Log 4 – Log 8 Pa·s) were made of the prepared solid right cylinder glass samples (6 mm in diameter and 35 mm in height) with faces fine-ground. The samples were placed between two parallel inconel plates protected with platinum foil. A load of 205 g, which was found to be adequate for deforming the solid right cylinder in the softening range, was applied to the glass while heating at the ASTM specified rate of 5 K min^{-1} [20]. The sample height was monitored as a function of temperature and used in the viscosity calculation as shown below [20]

$$\eta = 2\pi \frac{Mgh^5}{30V(dh/dt)(2\pi h^3 + V)},$$ (3.2)

where V is the specimen volume (cm^3) and h (cm) is the specimen thickness at time t (s).

Experimental errors of the beam bending measurements can be attributed to the confidence of the Type "S" thermocouple, which is approximately ±1°C, and the position of the thermocouple approximately 3 mm from the glass sample. However, the NIST 710a [49] was used as a standard glass with known viscosity values in the softening region to correct for any experimental error.

3.2 Structural Relaxation Instrumentation and Characterization

The structural relaxation of the investigated glasses was characterized by quantifying the thermal expansion and specific heat properties above, below and within the Glass transition region, as both the α and c_p have been discussed in relevance to the TNM model defining the kinetics of glass properties in the glass transition region.

3.2.1 Thermal expansion instrumentation

A thermo-mechanical analyzer TMA 2940 of TA instruments seen in Figure 3.5 was used to measure the thermal expansion as a function of temperature through the glass transition region [50].
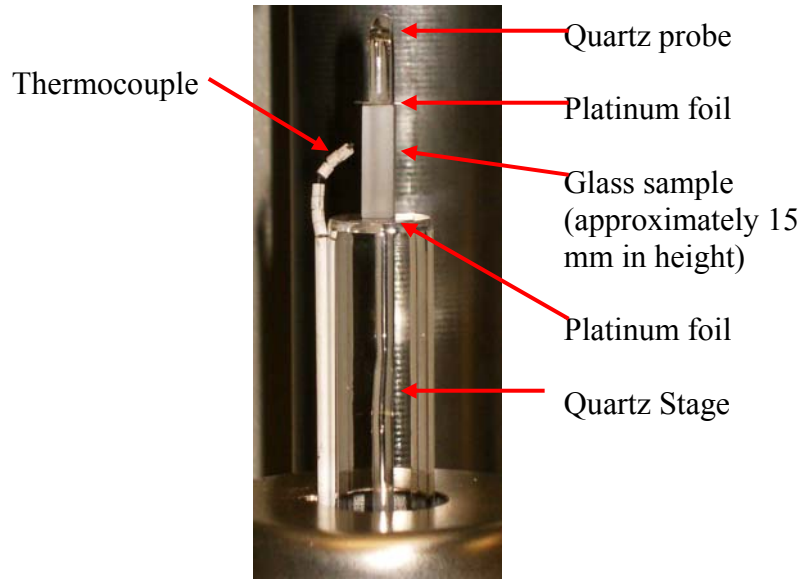
Figure 3.5: Glass sample loaded onto TMA sample stage.

The figure shows the glass sample (end faces polished and parallel) placed between the fused quartz stage and standard expansion probe which are both protected with 0.0254 mm thick platinum foil. The sample thermocouple resides as close as possible to the glass sample without touching. The TMA furnace can be raised for sample loading, and

lowered over the sample to run an experiment. The quartz probe measures the sample expansion with increasing temperature as it passes through the instrument LVDT. The TMA cell has a temperature range of -150 – 1000°C in an air atmosphere monitored by a type "K" sample thermocouple, which has a confidence of ± 1.5^{o}C at from room temperature to 375°C and changes linearly to ± 2.7^{o}C at 675°C, which was the maximum test temperature for our studies. The programmable rate of heating or cooling is 0.1 – 200 K min^{-1}. The fused quartz expansion probe has a sensitivity 100 nm with a ±2.5 mm displacement range. The force applied to the sample by the fused quartz probe can be controlled to range between 0.001 – 1 Newtons (0.102 – 102 g).

3.2.2   *Specific heat instrumentation and calibration*

A disc-type differential scanning calorimeter DSC 2920 of TA instruments was used to measure the specific heat as a function of temperature for different rates through the glass transition region [51]. Seen in Fig. 3.6 is the schematic for the DSC cell.
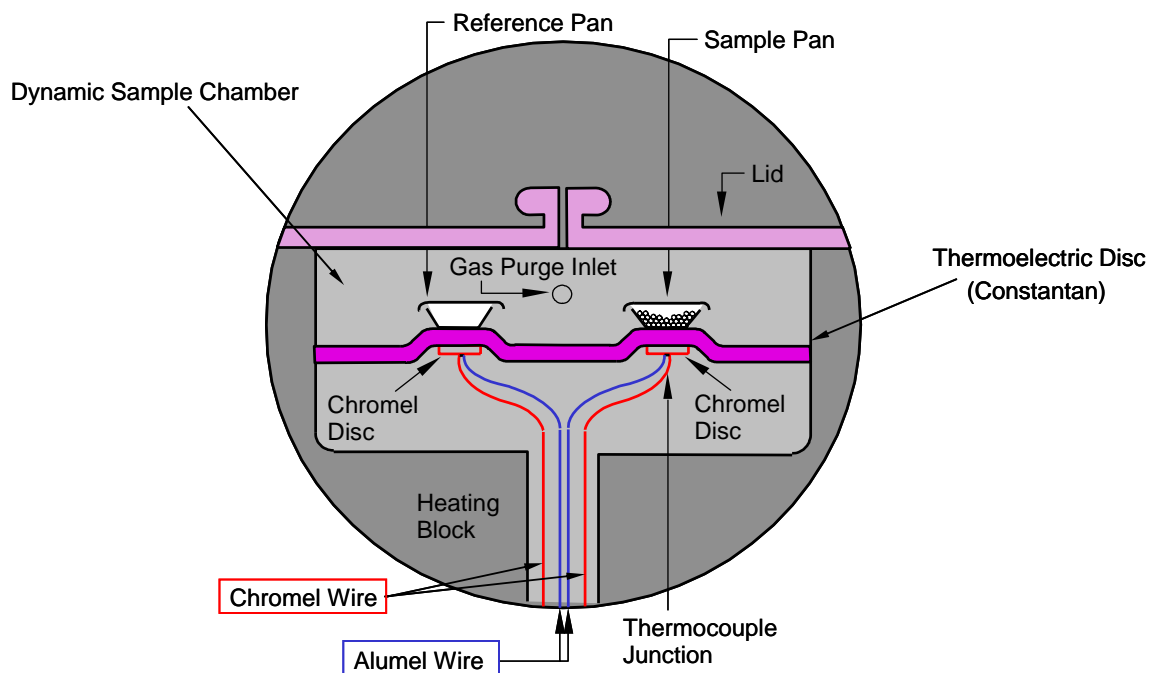
Fig. 3.6: Schematic of the DSC 2920 cell courtesy of TA Instruments.

The DSC 2920 contains two major parts, which are the instrument itself housing the system electronics, and the DSC standard cell, which contains thermocouples for monitoring differential temperature and operates in purged N_2 gas environment (95 cc min^{-1} flow rate). The sample and reference pans sit on raised platforms on a constantan disc that is resistively heated. Heat is transferred through the disc up into the sample and reference pans, while monitoring the differential temperature via thermocouple wires welded to the constantan disc. The CHROMEL®-constantan differential thermocouple (type "E") monitors the temperature difference between the sample and reference pan with a reported 0.2 μV (rms) sensitivity and 0.1 μV baseline noise. The differential temperature, ΔT, is measured as a function of the sample temperature monitored by the CHROMEL®-ALUMEL® sample thermocouple (type "K").

Calibration of the DSC cell involves two separate calibrations. The first calibration (explained in detail in **Appendix B**) is that of the sample thermocouple which monitors the temperature of the sample pan. This was done by measuring the temperature at which the onset of the melting peak of zinc (theoretical value T_m = 419.53^{o}C) occurs. To be as accurate as possible, a small hole (~1 mm diameter and 0.5 mm deep) was drilled into a glass disk sample (5.75 mm in diameter, 1 mm thickness, and the surface in contact with the bottom of the pan is polished), which was to be tested. A small piece of zinc wire (99.999% pure and 1 mm diameter, from Goodfellow) was placed into this hole and the glass/zinc sample into the platinum sample pan. The onset of the T_m of zinc was measured at 4 and 8 K min^{-1} scanning rates because these were the two heating rates used for analysis of the glass compositions. The difference between the measured value and the theoretical value for the rate of interest was used as the linear offset for calibrating the sample thermocouple.

Calibration of the differential thermocouples monitoring the temperature difference between the reference and sample pans in order to compute the c_p as a function of temperature was done by determining what time delay the measured ΔT is distorted, or "smeared". This is done by computing the time constant, τ_c, of the "backswinging" of the zinc melting peak (for more detail see **Appendix C**).

From the temperature and time constant calibration, the c_p of the glass is computed by making three separate runs (for more detail see **Appendix D**). Note that the temperature calibration described above was applied to all three of these necessary three DSC runs. The first scan measured the ΔT signal (units of μV) across empty sample and reference

pans creating a baseline to be subtracted from the following two measurements. The second scan measured the ΔT signal of a sapphire standard, ΔT_{st}, in the sample pan, with the reference pan empty, which was used to determine the thermal resistance R between the furnace and the platinum pan according to the following equation

$$R = \frac{-\Delta T_{st}}{c_{st} \cdot \dot{T} \cdot m} \qquad (3.3)$$

where c_{st} is the specific heat (J g^{-1} K^{-1}) of the sapphire obtained from [52], $\dot{T}$ is the heating rate (K s^{-1}), and m is the mass (g) of the sapphire. The third scan measured the ΔT signal of the glass sample, ΔT_{gl}, (5.75 mm in diameter, 1 mm thickness, and the surface in contact with the bottom of the crucible was polished) in the sample pan with the reference pan empty. The specific heat of the glass, $c_{p,gl}$ (J g^{-1} K^{-1}), as a function of temperature was calculated from the following formula [32, 53]

$$c_{p,gl} = -\frac{\Delta T_{gl} + \frac{d\Delta T_{gl}}{dT} \cdot \dot{T} \cdot \tau_c}{R \cdot \dot{T} \cdot m} \qquad (3.4)$$

where ΔT_{gl} is the differential temperature measured from the DSC (μV), $\frac{\Delta T_{gl}}{dT}$ is the temperature derivative of the differential temperature measured from the DSC (μV K^{-1}), τ_c is the determined time constant (s), R is the thermal resistance determined from equation (3.3), and m is the mass of the glass (g).

3.2.3   Experimental method

The glass samples used for analyzing expansion data were fabricated with a low-speed diamond saw (Buehler) to be approximately 4 x 4 x 15 mm with ends polished and

sides fine-ground. The polished ends of the glass sample were directly in contact with the platinum foil protecting the fused quartz stage and probe. The nominal force applied by the probe to the sample was controlled and maintained at 0.05 N. The expansion of the glass was then measured with the TMA 2940 of TA instruments as a function of temperature through the transition region at a heating rate of 2 K min^{-1} where the previous cooling rate was also 2 K min^{-1}. This was done to be consistent with the procedure that is followed by glass manufacturers when reporting the thermal expansion coefficient and even T_g values, which was learned by private communication with SCHOTT [54]. The thermal expansion coefficient of the glass was determined by differentiating the expansion curve with respect to temperature and dividing by the initial sample height. Isothermal measurements of glass expansion or contraction in the transition region were conducted following a temperature profile described by the figure below.
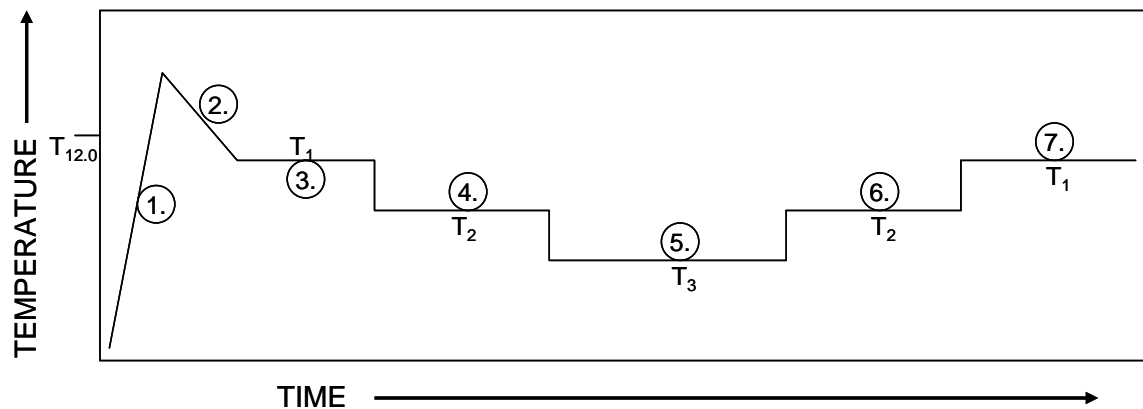
Figure 3.7: Experimental summary of isothermal TMA experiments.

The Fig. 3.7 shows temperature-time profile performed for isothermal measurements of glass expansion and/or contraction in the transition region. The temperature-time procedure consisted of seven steps:

1. The glass was heated at 5 K min^{-1} well above T_g.

2. The glass was cooled at 1 K min^{-1} to a temperature T_1 approximately 5°C below the annealing point temperature (viscosity of Log 12.0 Pa s) as to minimize any plausible sample deformation due to the controlled 0.05 N force of the probe.

3. The glass was equilibrated at a temperature T_1 for approximately 6 hours.

4. The glass was equilibrated at a temperature T_2 for 8 hours (decrease from T_1 to T_2 was 5°C).

5. The glass was equilibrated at a temperature T_3 for approximately 14 hours (decrease from T_2 to T_3 was 5°C).

6. The glass was equilibrated at T_2 for approximately 8 hours (increase from T_3 to T_2 was 5°C).

7. The glass was equilibrated at a T_1 for 6 hours (increase from T_2 to T_1 was 5°C).

It should be noted that the heating or cooling rate between steps for steps 3 − 7 was 5 K min^{-1} and the T_1 is approximately 5°C below the annealing point temperature, $T_{12.0}$, of the glass.

Glass samples for specific heat measurements were prepared by using a diamond core drill (Shibuya TS-092) to drill glass cores with a diameter of 5.75 mm. The glass cores were sliced with a low-speed diamond saw (Buehler) and then polished on one surface to have a thickness of approximately 1 mm. The glass samples were then annealed for

approximately 200 hours at a temperature, T_e, approximately 30°C below the annealing point temperature of the glass (the temperature corresponding to a viscosity of Log 12.0 Pa s) depending upon glass type. After equilibration, the samples were quenched by rapid removal from the furnace. The T_e was chosen to be high enough that sufficient time was allowed for equilibration but low enough that relaxation times were too slow for any relaxation to occur when the samples were quenched from the equilibration temperature to room temperature.

The DSC 2920 of TA instruments was employed to measure the specific heat, c_p, of glass as a function of temperature through the glass transition region. For each glass and each heating rate, both the temperature calibration (see above and **Appendix B**) and the differential temperature calibration (see above and **Appendix C**) were performed. The three essential runs for the differential temperature calibration were carried out such that each started with an isothermal hold at 100°C and ended with an isothermal hold at the maximum temperature. A correction, or rotation, was performed of the DSC signal with respect to the positions at the isothermal holds so that they were the same (for more details see **Appendix D**). The DSC signals obtained from the three runs were used to calculate the c_p of the glass as discussed above according to equation 3.4.

3.3 Numerical Simulation of the Tool-Narayanaswamy-Moynihan (TNM) Model

3.3.1   Development of numerical model

The mathematical software MATLAB was used to computationally solve the differential equations of the TNM model discussed in the previous chapter as they apply

to the thermal expansion and specific heat measurements. The development of the mathematical code was performed with the collaboration with Professor Chris Cox of the School of Mathematical Sciences at Clemson University. First, a mathematical routine was developed to integrate experimental c_p data in order to find the fictive temperature of the glass as a function of temperature. The code developed for solving the set of differential equations of the TNM model discussed in the previous chapter employed the 'ODE15s' ordinary differential equation solver of MATLAB, which is a multi-step solver used for 'stiff' differential equations – differential equations that would normally require very small step-sizes and thus long times of a numerical method to compute. Finally a code was written that optimized the four structural relaxation parameters H/k, x, β, and τ_0 by minimizing the sum of least squares between experimental and calculated data using the 'fminsearch' function in MATLAB.

3.3.2 Experimental method

The developed MATLAB code was used to follow the experimental flow chart seen in the Fig. 3.6 below.
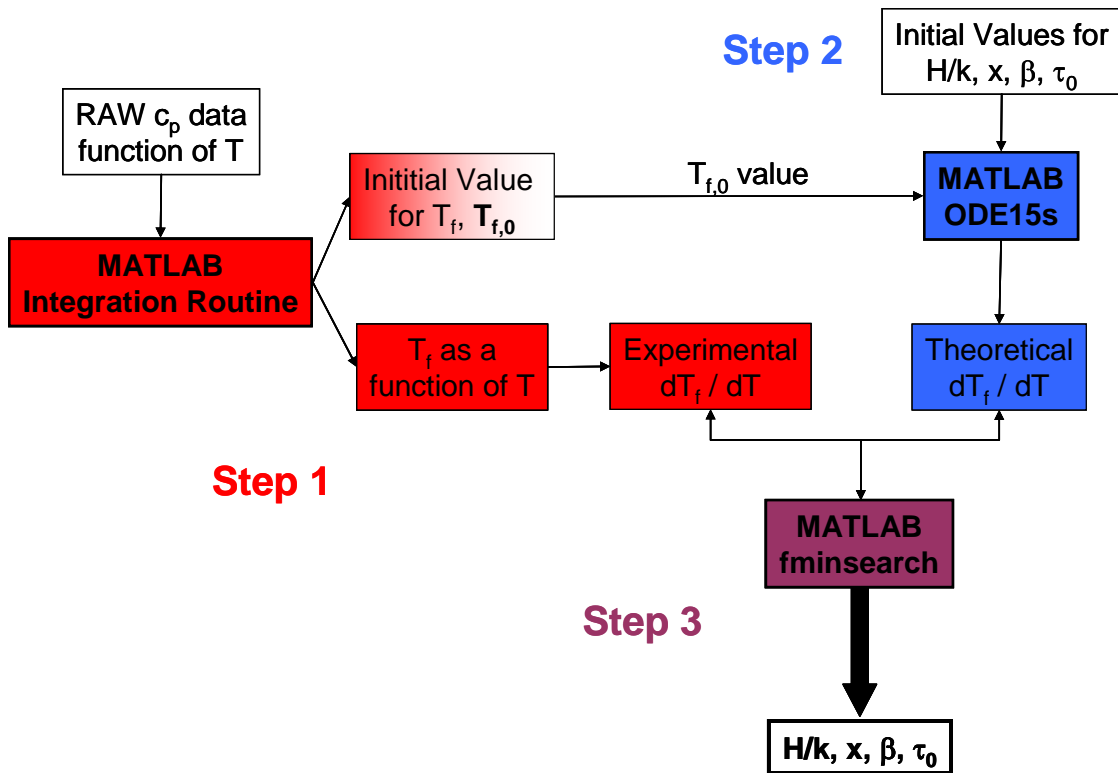
Fig. 3.8: Flow chart depicting the determination of the structural relaxation parameters from experimental c_p data.

The method was used to determine the four structural relaxation parameters and was divided into three separate and essential steps:

1. Find the fictive temperature as a function of temperature and the initial value of the fictive temperature, $T_{f,0}$, by integrating the c_p curve according to equation (2.6).

2. Solve the set of differential equations of the TNM model (equations (2.13-2.17)) for given structural relaxation parameter values of H/k, x, β, and τ_0 and an initial value of the fictive temperature, $T_{f,0}$.

3. Optimize the four structural relaxation parameters to minimize the sum of least squares between the experimental and calculated data.

The experimental c_p data was divided into temperature increments of 0.5°C and imported to the integration routine. The specified boundary conditions were the value of $c_{p,l}$ just above the transition region where it can be assumed that $T_f = T$ and the value of $c_{p,g}$ at a temperature below the transition region where it can be assumed that T_f does not change with changing T. The integration according to equation (2.6) provided the experimentally determined $T_{f,0}$ – which was confirmed to be equal to the T_e of the glass sample – and the experimental data for the T_f as a function temperature, T. The derivative of this data with respect to temperature resulted as the experimentally determined dT_f / dT. The ODE15s function in MATLAB used the experimentally verified $T_{f,0}$ value and starting values for the four structural relaxation parameters as inputs to compute the theoretical curve for dT_f / dT. A time-step was chosen that would coincide with the temperature step of 0.5°C, which was 3.75 s and 7.5 s for 4 and 8 K min^{-1} respectively. The 'fminsearch' function optimized the H/k, x, β, and τ_0 values such that the sum of the least squares between experimental and theoretical data points were minimized.

This thesis shows the development of a method to characterize important glass properties that need to be determined for modeling the glass response to the PGM process. Experimental techniques were developed here at Clemson University to characterize the following key material properties for each glass type:

1. Glass viscosity constants (A, B, and T_0) to the VFT equation to define the temperature range for molding (Log 8.0 – Log 6.6 Pa s).

2. Thermal expansion properties in the glassy (α_g) and liquid states (α_l).

3. Structural relaxation parameters (E/R, x, β, τ_0) of the TNM model.

The glass viscosity was directly measured in the annealing and softening range by beam-bending and parallel plate viscometers respectively. The VFT viscosity equation was used to interpolate viscosity data that defined an appropriate temperature region for molding. The method of determining the thermal expansion properties before and after the transition region was performed. Lastly the structural relaxation properties were determined by curve-fitting precise c_p measurements so that the thermal expansion coefficient of the glass could be modeled as a function of rate through the glass transition region. The results of these measurements and their impact on our program goals are discussed in the following chapter.

CHAPTER FOUR

RESULTS AND DISCUSSION

As explained in Chapters One and Two, the PGM process involves exposing (heating) the glass to temperatures above T_g at a specific and appropriate molding temperature in the range of Log 8.0 – Log 6.6 Pa s, pressing the glass into a precise lens shape, and then cooling rapidly back to room temperature for removal from the mold. However, when the glass is cooled to be removed from the mold, the lens shape is different than that which was molded at the molding temperature due to stress and structural relaxation. In order to develop an adequate model of the glass response to the molding process for each glass type, an appropriate range of temperatures must be defined as well as a thermal expansion model including expansion (or contraction) behavior, above, below, and within the glass transition region.

The viscosity, or resistance to flow, of glass must be known when defining a molding temperature. At high viscosities (low temperatures), a large force is required to press the glass blank into the desired lens shape. This can often result in cracking of the glass because of its brittle nature if performed at too low a temperature. At lower viscosities (higher temperatures) the glass is less viscous, and after cooling, the glass may stick to the mold material. The lower-bound of the molding temperature range has been discussed to be at a temperature where the glass begins to deform under its own weight, which occurs at a viscosity of approximately $10^{8.0}$ Pa s [4, 5]. The temperature corresponding to a viscosity $10^{6.6}$ Pa s ($T_{6.6}$) has been typically discussed as the upper-

bound of the molding temperature range. The difference in temperature (T_Δ) at these viscosity values range greatly depending upon glass chemistry and structure; as discussed in Chapter Three and shown in Fig. 2.2, these material attributes dictate the kinetic fragility of the glass' viscosity (large T_Δ for strong glasses and smaller ΔT for fragile glasses). These attributes are analogous to historically used definitions of "long" and "short" glasses, which refer to the temperature range over which a material is "workable". The Table 4.1 below shows the measured T_Δ for the investigated glasses.

Table 4.1: Measured T_Δ for N-BK7, P-SK57, and L-BAL35.

Glass Type	T_Δ (°C)
N-BK7	60 → strong
P-SK57	49 → fragile
L-BAL35	45 → fragile

Once the T_Δ of the glass is defined, a thermal expansion model must be developed in order to predict lens size and shape change as a function of the molding process – specifically the cooling profile. Seen below is a schematic showing the behavior of the thermal expansion coefficient of glass upon cooling from temperatures above the T_g region where molding takes place.
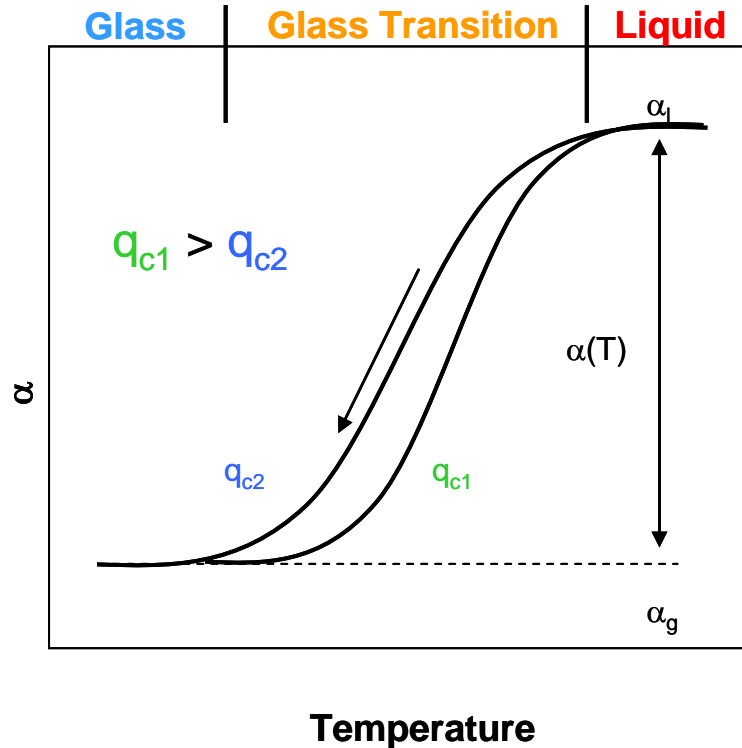
Fig. 4.1: Schematic of the behavior of the thermal expansion coefficient of a glass upon cooling from the liquid state through the glass transition region.

The Fig. 4.1 is shown to indicate the three specific aspects of a thermal expansion curve (in this case upon cooling from the liquid state): *i)* constant expansion in the liquid state quantified by α_l, *ii)* non-linear, rate-dependent path ($\alpha(T)$) for which the α_l value transitions to the glassy state, and *iii)* constant expansion in the glassy state quantified by α_g. Note that if interpreted with respect to volume, the integral of the curve in Fig. 4.1 would be well-represented by the schematic shown in Fig. 2.1 ($\alpha(T)dT = \dfrac{dV}{V_0}$). The α_g value can be easily determined from rate-heating dilatometric techniques. However, the α_l and $\alpha(T)$ are difficult to determine directly from dilatometry due to the fact that there is some nominal force applied by the probe to the sample, which deforms the soft glass within and above the glass transition region. The α_l can be carefully estimated by

isothermal measurements, but the behavior of $\alpha(T)$ through the transition region is best determined from studying the enthalpic response of glass (quantified by specific heat, c_p, measurements) as a function of temperature and rate as it has been found that for most borosilicates and soda-lime-silicates the kinetics of enthalpy and volume relaxation are experimentally indistinguishable [32, 33, 44].

From precise c_p measurements, the TNM model can be applied to determine the four structural relaxation parameters that, for some glass types, universally describe the enthalpic and volumetric relaxation of glass within the glass transition region. This is done by performing non-linear curve-fitting routines to c_p data according to equations of the TNM model described in Chapter Three.

Within the results of this thesis is shown a method for determining an appropriate range of temperatures for lens molding by determining the viscosity-temperature curve from the annealing to softening ranges of the glass. Secondly, a way is shown to develop a thermal expansion model by determining each of the three aspects of the thermal expansion curve (see Fig. 4.1) separately: *i)* the α_g determined by rate-heating dilatometric measurements, *ii)* the α_l determined by isothermal expansion and contraction measurements in the transition region, and *iii)* and the $\alpha(T)$ determined by the application of the TNM model to c_p measurements

4.1 Glass Viscosity

The viscosity of N-BK7, P-SK57, and L-BAL35 glass types was measured by beam-bending and parallel-plate viscometers in order to define the viscosity in the annealing and softening ranges of the glass, respectively. In the annealing range, the viscosity was measured as a function of time at an isothermal temperature with the beam-bending viscometer as within this low-temperature region, the relaxation kinetics are expected to be slow, and therefore some time must be allowed for the glass viscosity to reach its equilibrium value [10]. Within the softening range, the measurement temperatures are well above the Glass transition region, and therefore the relaxation processes are expected to be instantaneous [55, 56]. For this reason, viscosity measurements made at a heating rate of 5 K min^{-1} with the parallel-plate viscometer reproduce well the equilibrium glass viscosity in the softening region of the glass.

Routine (weekly) measurements of P-SF67 glass in our laboratory were performed as a reference test material compared to viscosity data calculated from A, B, and T_0 constants provided by SCHOTT [28]. It was found that within the annealing region of the glass (Log 13.0 − Log 11.0 Pa s), isothermal measurements of P-SF67 reproduced well the Log viscosity (± 0.2 Pa s) information provided by the vendor, which validated the measurement technique and instrumentation.

Fig. 4.2 shows the midpoint displacement of an N-BK7 glass beam as a function of time measured with the BBV-1000 at 570°C
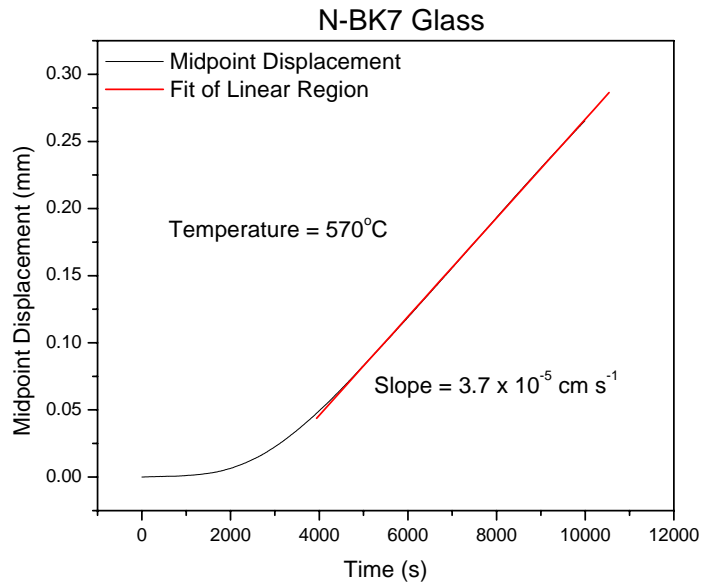
Fig. 4.2: Isothermal beam midpoint deflection of N-BK7 glass measured as a function of time.

The Fig. 4.2 above shows the midpoint displacement of the glass beam upon the application of a 360 g load to the midpoint of a N-BK7 glass beam at 570°C (a temperature that corresponds to 13°C above the SCHOTT-reported T_g of 557°C). It should be noted here that aside from measuring the viscosity of a glass with known values, no extensive temperature calibration was performed throughout the ranges of test temperatures. Therefore, the temperature gradient inside the furnace and its dependence upon temperature is not precisely known. The figure shows that just after the initial application of the load (time = 0 s), the response of the midpoint displacement is very slow. However, as time progresses, the midpoint displacement rate increases as a function of time. During this progression of time, both stress relaxation and structural relaxation mechanisms contribute to the material response to a constant load at an

isothermal temperature. As the derived equation (3.1) for the calculation of viscosity describes the steady state only, the displacement data seen in Fig. 4.2 is not used for computing the viscosity until the displacement rate remains constant. The midpoint displacement rate can be seen to reach a constant value in Fig. 4.2 after approximately one hour indicating that the glass has reached steady state. A linear fit was applied to the midpoint deflection data after the first hour of measurement to determine the constant equilibrium displacement rate (3.7×10^{-5} cm s^{-1}) used to compute the viscosity at 570°C using equation (3.1). The equilibrium viscosity value at 570°C for N-BK7 was found to be Log (12.1 ± 0.2) Pa s.

Isothermal, equilibrium viscosity measurement results were made of N-BK7, P-SK57, and L-BAL35 such that the target test temperatures were at a Log viscosity of approximately 12.0 Pa s. This was done due to the fact that at higher viscosities the test time is very long, and at lower viscosities, the glass beam geometry deforms very quickly and results in compromised viscosity calculations which are made with specific geometrical inputs (see equation (3.1)) assumed to be constant. The results for isothermal beam-bending measurements made of the investigated glasses at the target test temperature that closely corresponded to a Log viscosity of 12.0 Pa s are shown in the Table 4.2 below.

Table 4.2: Isothermal beam-bending viscosity measurements made of N-BK7, P-SK57, and L-BAL35 glass types.

	Isothermal Test Temperature	Log Viscosity (Pa s)
N-BK7	570°C	12.1 ± 0.2
P-SK57	486°C	12.2 ± 0.2
L-BAL35	523°C	12.2 ± 0.2

The measurements shown in Table 4.2 indicate the position of the viscosity curve with respect to temperature for all three investigated glass types. The table shows that for a specific viscosity in the annealing range shared for all three glass types, the viscosity value for N-BK7 is at the highest temperature and for P-SK57 the lowest temperature.

Before measuring the viscosity of the glasses within this study, a NIST 710a glass sample was first measured and compared to published data. From the NIST sample, a temperature offset of (-2°C) was found between the measured and accepted viscosity data and this offset was applied to subsequent measurements of the investigated glasses. The PPV instrument measurement of an N-BK7 glass disk sample is shown below.
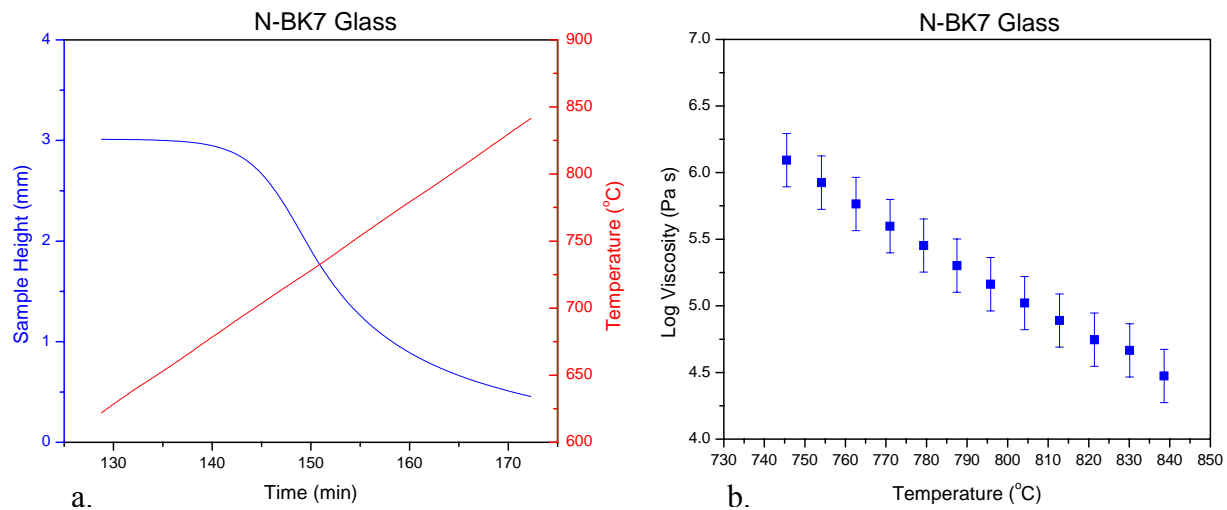
Fig. 4.3: The sample height deformation as a function of time of an N-BK7 glass disk upon heating 5 K min^{-1} (a), and the calculated viscosity from the measured height deformation rate (b).

Fig. 4.3a shows the direct measurement of the sample height deformation as a function of time upon increasing temperature at 5 K min^{-1}. From the sample deformation data, the rate of deformation with respect to time can be calculated. The sample deformation rate (cm/s) was used to then compute the viscosity as a function of temperature according to equation (3.2). Fig. 4.3b shows the result of the calculations of equation (3.2) by plotting the Log viscosity (Pa s) as a function of temperature (^{o}C) with the indicated accuracy of the measured Log viscosity to be ($\pm$ 0.2 Pa s). It was found through measurements of the NIST glass and the investigated glasses, that the viscosity measured in the range of Log 4.0 − Log 6.0 Pa s best reproduces published values within the accuracy of the measurement, even though higher viscosity values could mathematically be calculated (up to viscosity values of Log 9.0 Pa s). The measured viscosity results in the softening region of the glass for all three investigated glass types are shown below.
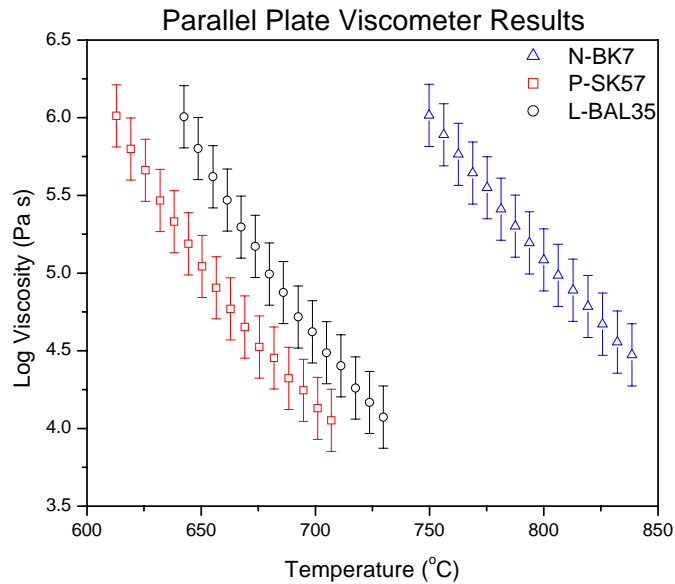
Fig. 4.4: Log viscosity as a function of temperature determined from the parallel plate viscometer for N-BK7, P-SK57, and L-BAL35 glass types.

The results shown in Fig. 4.4 reveal similar results as shown in Table 4.2. The viscosity of N-BK7 glass is at the highest temperatures, while that of P-SK57 is at the lowest temperatures with respect to the three investigated glass types. Over the range of temperatures shown in Fig. 4.4, the slope of the viscosity curves of the investigated glasses is difficult to differentiate among one another. Within the accuracy of the measurement, the change in viscosity with respect to equal changes in temperature is the same. However, as shown below in Fig. 4.5, when combined with the lower temperature viscosity data, the degree to which the viscosity depends upon temperature is more easily seen. The compiled viscosity curves of the three glasses are shown in the figure below.
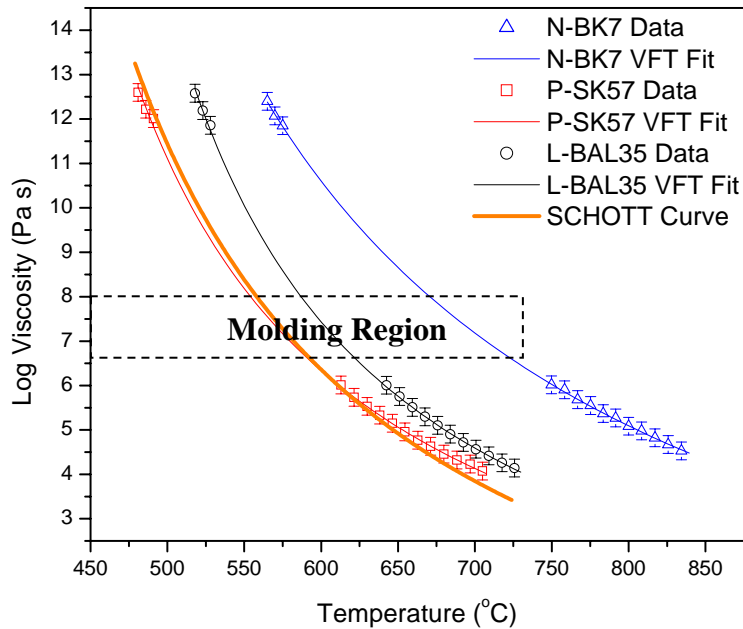
Figure 4.5: The compiled viscosity curves in the annealing and softening regions of N-BK7, P-SK57, and L-BAL35 glasses.

The Fig. 4.5 shows the compiled annealing range and softening range viscosity measurements made for N-BK7, P-SK57, and L-BAL35 glasses. The data points were fit to the well-known VFT equation (2.2), which is indicated by the solid line in Fig. 4.5. It is not precisely known why the temperature corresponding to a Log viscosity of 12.0 Pa s for N-BK7 was found to be nearly 570°C when the SCHOTT reported value is 557°C. As mentioned earlier, no extensive temperature calibration was performed of the sample thermocouple, and therefore could very well be the reason for the noted discrepancy for N-BK7 glass. However, at approximately 100°C below the testing temperature in the annealing region for N-BK7, the solid orange line shows the viscosity information

provided by SCHOTT for P-SK57, and our experimental data in the annealing region does in fact coincide within experimental error with the data determined at SCHOTT. Since neither the temperature gradient, nor its dependence upon temperature is known, it is likely that at higher temperatures where our measurements are made for N-BK7 glass, the apparent temperature is less accurate than in the temperature region where glass viscosity measurements in the annealing region are made for both P-SK57 and L-BAL35. In addition to our ability to repeat viscosity data in the annealing region for P-SK57, Fig. 4.5 also shows the viscosity data determined in the softening region via the parallel-plate technique is also in good agreement with data determined internally for P-SK57 at the glass manufacturing company, although they do not measure viscosity the same way. In fact, it was learned through private communication that the VFT equation producing the SCHOTT curve in Fig. 4.5 was determined from the measurement of viscosity-temperature data points using three techniques described below [57]:

1. Multiple viscosity-temperature data points are obtained in the annealing region by an isothermal, three-point bending technique similar to what was discussed above.

2. Multiple viscosity-temperature data points (temperature corresponding to Log 6.6 Pa s) is obtained in the softening region by measuring the elongation of a glass fiber at a 5 K min^{-1} heating rate.

3. Multiple viscosity-temperature data points are obtained in the molten glass region at isothermal temperatures using a rotating spindle (approximately Log 3.0 – less than Log 1.0 Pa s).

The VFT curve-fit between data points shown in Fig. 4.5 was used to interpolate the viscosity of Log 8.0 – Log 6.6 Pa s defining the molding range of the three glass types. Table 4.3 shows the constants to the VFT equation calculated using equation (2.2) for the investigated glass types as well as the molding temperature range determined from the VFT constants to be at temperatures corresponding to the viscosity range of Log 8.0 – Log 6.6 Pa s.

Table 4.3: Constants to the VFT equation (2.2) determined from data shown in Fig. 4.5 used to compute the appropriate molding region at temperatures corresponding to the viscosity range of Log 8.0 – Log 6.6 Pa s.

	A	B	T_0	Molding Temperature Range
N-BK7	-3.52	4419	287	664 – 732°C
P-SK57	-1.85	2224	328	549 – 598°C
L-BAL35	-1.90	2128	372	583 – 628°C

The Table 4.3 in conjunction with the Fig. 4.5 shows that the N-BK7 glass has a viscosity curve at higher temperatures (and thus a molding temperature range at higher temperatures). For this reason, N-BK7 glass may be referred to as a "higher-temperature" glass, meaning that specific thermo-rheological characteristics are at higher temperatures than P-SK57 and L-BAL35. It is not precisely known the chemical composition of the investigated glass types, but N-BK7 is presumed to be similar in composition to the borosilicate BK-7 glass [35]. Typically, Nb and Ti or Ta are added to "N" type glasses to maintain index and dispersion values when ingredients are removed, but this is most significant in the case of flint glasses (containing Pb) and not prevalent in

silicate materials. P-SK57 is a silicate glass likely similar to L-BAL35 and probably differing only in glass-former content (silica). If this assumption is valid, it can be inferred from Fig. 4.5 and Table 4.3 that P-SK57 likely contains less glass-former content (and thus, more alkali- or alkaline earth-oxide or intermediate content) than L-BAL35. By increasing alkali content in a largely silicate-based glass composition, the well-interconnected, covalently-bonded silicate network is disrupted. As weaker ionic bonds are introduced, non-bridging oxygen atoms are also incorporated into the glass network. Therefore, the presumed weaker bonding and non-bridging oxygens within the glass network likely result in the shift of the viscosity curve to lower temperatures [4, 58] for P-SK57 compared to L-BAL35. In a similar way, N-BK7 is a borosilicate glass, whose viscosity curve is shifted to higher temperature as compared to P-SK57 and L-BAL35. This shift is most likely due to the known incorporation of borate groups and possibly less alkali content than the other two glass types. Therefore, for purposes of our study, P-SK57 and L-BAL35 glasses can be termed "lower-temperature" glasses with respect to N-BK7 and thus, the subsequent molding temperature regions are lower than that of N-BK7.

The activation energy for viscous flow, E_η, in the range of Log 9.0 – Log 12.0 Pa s can be estimated from equation (2.1 and 2.2) for which the interpolated viscosity (from the VFT parameters in Table 4.3) is plotted in the figure below.
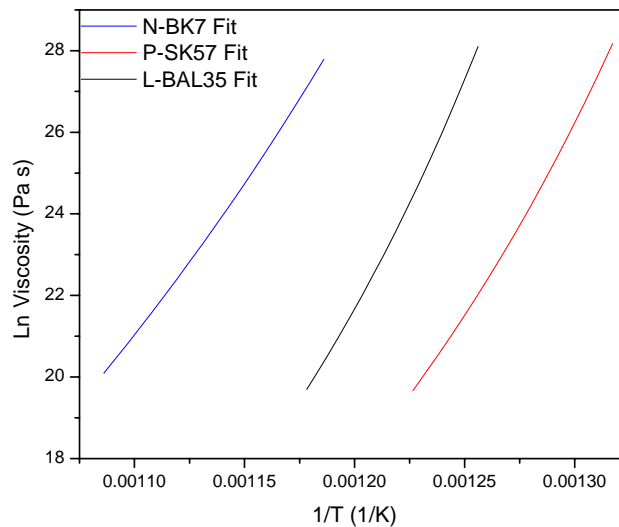
Fig. 4.6: Arrhenius plot of the viscosity versus 1/T between Log 12.0 – Log 9.0 Pa s.

Fig. 4.6 does in fact show the Arrhenius relationship between viscosity and temperature in the range of Log 12.0 – Log 9.0 Pa s, which indicates that over this viscosity range (and temperature range) the activation energy can be assumed constant determined from the slope of the Ln viscosity versus (1/T) curve using equation (2.1 and 2.2). The E_η was found to be (639 ± 17) kJ mol^{-1} for N-BK7, (776 ± 20) kJ mol^{-1} for P-SK57, and (891 ± 14) kJ mol^{-1} for L-BAL35. Using the determined E_η value from Fig. 4.6 and equation (2.1) and the T_{12} value (temperature corresponding to a viscosity of $10^{12.0}$ Pa s) calculated from the VFT constants in Table 4.3, the kinetic fragility (equation (2.3)) was found to be (40 ± 1) for N-BK7, (54 ± 1) for P-SK57, and (58 ± 2) for L-BAL35. The fragility parameter values with respect to glass type can be explained for the same reasons the viscosity curve of N-BK7 is shifted to higher temperatures than the other glass types. The glass network of the borosilicate glass is presumed to be more

well-interconnected than P-SK57 and L-BAL35 likely due to the incorporation of borate groups. If the assumption of a more covalently-bonded glass network is correct, a lower activation energy for viscous flow, E_η is observed and likewise the glass possesses a lower kinetic fragility than the other two glass types. Indicating the degree to which the viscosity is dependent upon temperature, the kinetic fragility indicates that the N-BK7 glass network is more 'strong' than that of P-SK57 or L-BAL35. The determined fragility parameter explains why the viscosity curve of N-BK7 glass is more "flat" [less steep] than the other two glass types, which results in less of a change of viscosity with equal change in temperature compared to P-SK57 and L-BAL35. The fragility parameter values also reflect the temperature range calculated for molding as both P-SK57 and L-BAL35 glasses appear to have an equal magnitude of temperatures within the molding range, and N-BK7 glass has a much larger range of temperatures that correspond to a viscosity range of Log 8.0 – Log 6.6 Pa s.

4.2 Structural Relaxation

The thermal expansion and specific heat properties of N-BK7, P-SK57, and L-BAL35 glasses were measured in order to determine three aspects of the thermal expansion behavior of glass:

1. The thermal expansion coefficient below the glass transition region in the glassy state, α_g.

2. The thermal expansion coefficient above the glass transition region in the liquid state, α_l.

3. The heating/cooling rate-dependent path in which the thermal expansion coefficient (or specific heat) changes, or transitions, from the glassy to the liquid state, or visa versa.

Thermal expansion properties in the glassy state were determined by standard dilatometric techniques measuring the height expansion of a glass sample upon heating. Long-time isothermal experiments were conducted in the glass transition region in order to estimate the thermal expansion coefficient of the equilibrium liquid. Finally, the specific heat of the glasses was measured to determine the precise rate-dependent path the enthalpy (or volume under the assumption that the enthalpy and volume relaxation kinetics are the same) takes from the glassy state to the liquid state.

4.2.1 Thermal expansion properties

The Fig. 4.7 shows these results of the linear thermal expansion of the investigated glasses.
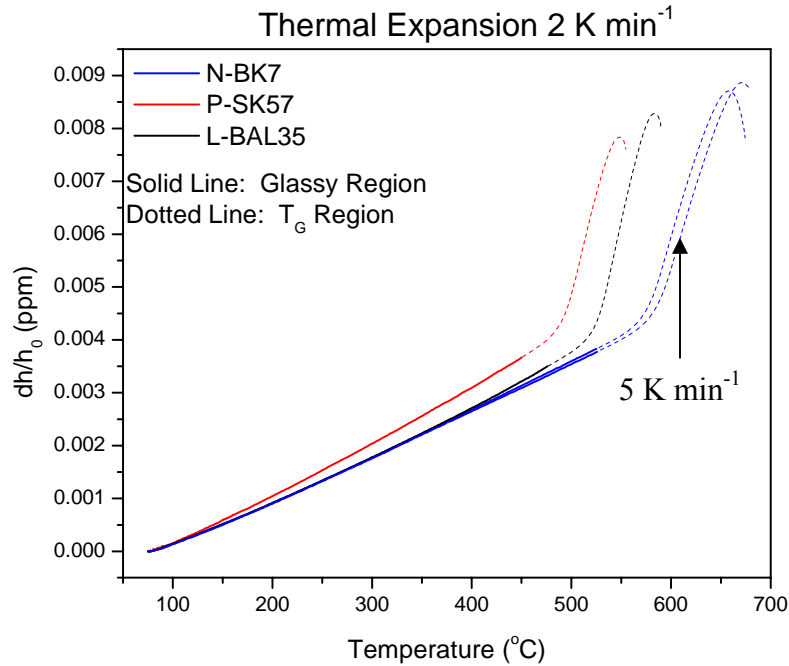
Fig. 4.7: Thermal expansion curve normalized to the original sample height (h_0) of N-BK7, P-SK57, and L-BAL35 glass types measured through the glass transition region at 2 K min^{-1}. The same thermal expansion curve measured at 5 K min^{-1} is also shown for N-BK7.

The Fig. 4.7 shows how the glass linearly expands in the lower temperature regime below the glass transition region. The linear change in sample dimension with respect to a change in temperature is what is referred to as the glassy thermal expansion coefficient, α_g. The figure shows that the α_g value is approximately constant, and it was calculated from the slope of the thermal expansion line shown in Fig. 4.7 from 100 – 300°C (well below the Glass transition region). The thermal expansion coefficient in the glassy state was found to be $(8.2 \pm 0.1) \times 10^{-6}$ K^{-1} for N-BK7, $(9.2 \pm 0.1) \times 10^{-6}$ K^{-1} for P-SK57, and $(8.2 \pm 0.1) \times 10^{-6}$ K^{-1} for L-BAL35. It was found that these values are in agreement with the values for N-BK7 reported by SCHOTT (8.3×10^{-6} K^{-1}) and L-BAL35 reported by

OHARA (8.1×10^{-6} K^{-1}). However, the determined α_g value for P-SK57 was found to be slightly higher than that which is reported by SCHOTT (8.9×10^{-6} K^{-1}). This discrepancy could be due to the fact that our determination of the α_g value was from $100 - 300^{\circ}$C whereas SCHOTT reports the thermal expansion coefficient from $20 - 300^{\circ}$C. While typically ignored due to such a small influence, it is known that the α_g does have a slight, linear temperature dependence ($\alpha_g = A + BT$; where B is on the order of 10^{-9}). This may in fact result in a slightly different value reported by SCHOTT as compared to the measurements in our laboratory. Multiple measurements were made in the glassy regime at varying heating rates, and as the curve plotted for N-BK7 at 5 K min^{-1} shown in Fig. 4.7 confirms, the α_g value is not dependent upon the heating rate as it is an instantaneous vibrational response of atoms to an increase in temperature well below T$_g$.

As the glass is heated beyond the glassy regime and into the glass transition region, the expansion of the glass begins to be affected by parameters other than the atomic *vibrational* contribution (quantified as α_g). Fig. 4.7 shows that as the glass enters the T$_g$ region, a thermally activated *configurational* rearrangement of atoms begins to contribute in addition to the vibrational response. The equation describing the vibrational and configurational behavior was modified from equation (2.4)

$$\frac{dh}{h_0} = \left(\alpha_l - \alpha_g\right)dT_f + \left(\alpha_g\right)dT \tag{4.1}$$

where dh is the change in sample height and h$_0$ the original sample height. Therefore, the α_l and α_g values are *linear* (as opposed to volume in equation (2.4b)) thermal expansion coefficients. Within the glass transition region a configurational contribution (quantified

as $\Delta\alpha = \alpha_l - \alpha_g$) begins to effect glass behavior. As equation (4.1) indicates, the Fig. 4.7 should reveal that as the glass is heated through the transition region (after which $dT_f = dT$), it should begin to expand linearly according to the α_l value. Instead, it can be seen that the glass begins to deform under its own weight (the force of the probe is controlled to be 0.05 N) noted at the maximum of the thermal expansion curve. It is reasonable to assume then that precise data within the transition region (dotted line of Fig. 4.7) depicting the kinetic behavior of the glass expansion is distorted in some way by the force of the probe, and therefore cannot be used.

Equation (4.1) indicates however, that if both the dT_f and dT are equivalent and held constant, the α_l value can be estimated. For isothermal test experiments, the change in temperature happens relatively instantaneously, while the time required for an equal change in fictive temperature is much longer in the glass transition region. Therefore, long-time isothermal tests in the glass transition region must be done in order for the change in T_f and T to be equal. The isothermal relaxation of T_f was measured by observing *i)* the glass contraction at a temperature T_2 after an equilibration at a temperature T_1 (5°C above T_2), and *ii)* the glass expansion at T_2 after an equilibration at the temperature T_3 (5°C below T_2). The T_2 was chosen to be at temperatures where deformation of the glass sample due to the probe could be minimized by being below temperatures corresponding to a viscosity of $10^{12.0}$ Pa s, but also high enough so that reasonable times were sufficient for relaxation to the glass' equilibrium state. Fig. 4.8 below shows these results during isothermal tests performed for N-BK7, P-SK57, and L-BAL35 glasses.
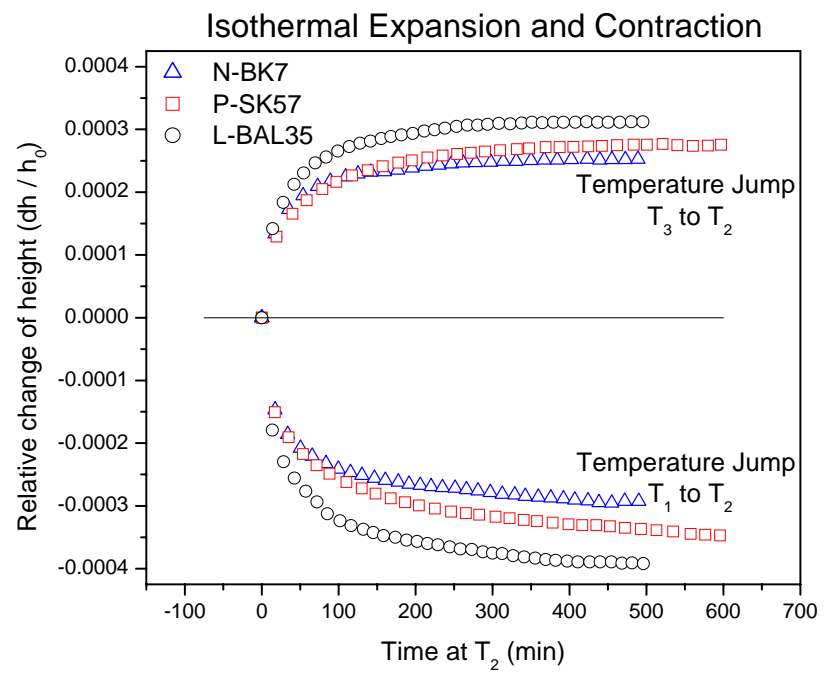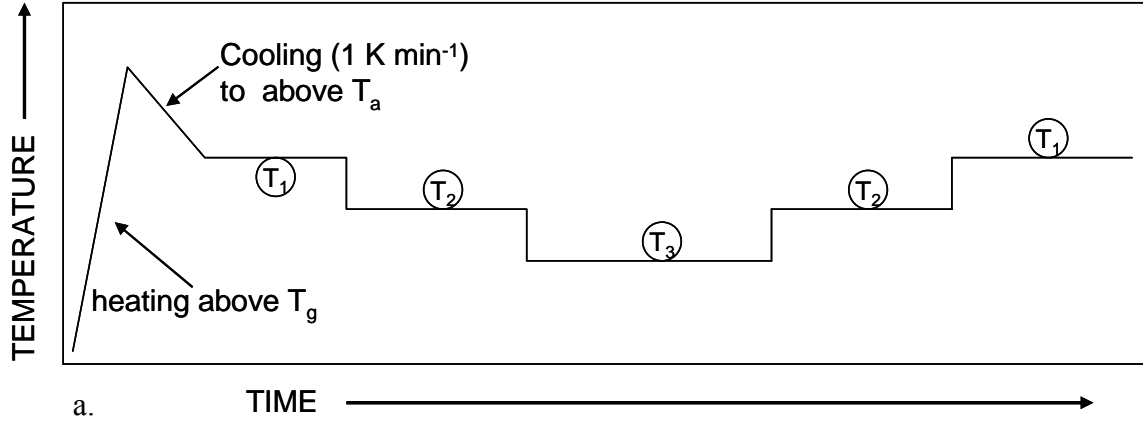
Fig. 4.8: Isothermal dilatometric experimental procedure (a) and isothermal expansion and contraction measurements at the temperature T_2 for N-BK7, P-SK57, and L-BAL35 glasses (b).

The figure above shows the isothermal expansion and contraction of the investigated glass types at the temperature T_2, which was 562, 475, and 515°C for N-BK7, P-SK57, and L-BAL35 glasses, respectively. The relaxation of the glasses at T_2 after a temperature-jump from T_3 and T_1 were equal in magnitude (5°C), but opposite in

direction. Furthermore, as no further glass sample relaxation was indicated by the isothermal expansion and contraction measurements at T_2 after 500 min, it can be determined that the change in T_f is equal in magnitude to the temperature-jump (5^oC). As one might expect, if deformation of the glass sample caused by the probe occurs upon relaxation from T_1 to T_2, the sample may appear to contract more than reality. Likewise, upon relaxation from T_3 to T_2, the sample may appear to expand less than reality. However, as it was shown in Fig. 4.5 that the viscosity curve of the three glass types differs for each, the 5^oC temperature jump experiments may not in fact correspond to an equal change in viscosity. Consequently, it may be more accurate to carry out isothermal contraction measurements where the *change in viscosity* for each 'jump' experiment is the same, rather than a *change in temperature*. This modification to the experiment may result in maintaining similar glass sample deformation due to the probe between all glass compositions. For the purposes of the above experiment, the change in temperature maintained at 5^oC was assumed to be small enough that the resulting differences of the change in viscosity may be neglected. Future experiments could be improved by such consideration as noted.

With this consideration it is not unreasonable to think that the magnitude of the glass response to an equal change in T_f and T has a value between that of the temperature "up-jump" and "down-jump." In fact, Fig. 4.7 shows that the difference between the magnitude of change between the up-jump and down-jump measurements for a single glass composition ranged between $[(43 - 84) \pm 0.05]$ ppm depending upon the glass type. Therefore, an estimate of a realistic change in normalized height (dh/h_0) of the glass

sample may be taken as the average between what was observed from the down-jump and up-jump measurements for a single glass type. These results are shown below in Table 4.4.

Table 4.4: Thermal expansion coefficient of the glassy state, average change of the glass normalized sample height (dh/h_0) between down-jump and up-jump isothermal relaxation experiments and the resulting linear α_l values for N-BK7, P-SK57, and L-BAL35.

	Fig. 4.7	**Fig. 4.8**		
	α_g (ppm K^{-1})	Relative Height Change (dh/h_0) (ppm)	α_l (ppm K^{-1})	$\Delta\alpha$ ($\alpha_l - \alpha_g$) (ppm K^{-1})
N-BK7	8.2 ± 0.1	271 ± 5	54 ± 1	46 ± 1
P-SK57	9.2 ± 0.1	312 ± 5	62 ± 1	53 ± 1
L-BAL35	8.2 ± 0.1	349 ± 5	70 ± 1	62 ± 1

By assuming that $dT_f = dT$ after the long-time isothermal experiments shown in Fig. 4.8, equation (4.1) becomes

$$\frac{dh}{h_0} = (\alpha_l)dT_f = (\alpha_l)dT \, , \tag{4.2}$$

and therefore, the α_l values were calculated as shown in Table 4.4. The thermal expansion results determined do not appear to be unreasonable as, for a soda-lime-silicate glass, α_l has in the past been accepted to be approximately $3 - 5$ times greater than α_g [10]. In 1999, Fotheringham *et al* discussed the characterization of a BK-7 glass (comparable optical properties to N-BK7), where the α_l was said to be 4.5 x 10^{-5} K^{-1} [31]. Furthermore, the results of Table 4.4 show that N-BK7 glass has less of a long-time dimensional thermal response to an equal change in temperature in the glass transition region than both P-SK57 and L-BAL35.

By the determination of the α_l values, more insight into the behavior of the thermal expansion coefficient through the transition region as functions of time and temperature is given. As the α_g for the investigated glass types are very close in value (see Fig. 4.6) and significantly different values for $\Delta\alpha = \alpha_l - \alpha_g$ were observed, the behavior of the precise relaxation kinetics that defines the apparent thermal expansion coefficient, $\alpha(T)$, through the glass transition region remains unknown. In order to precisely understand the time and temperature dependent path at which the glass transitions from the glassy state to the liquid state ($\alpha(T)$), a measurement technique must be employed that can cover the entire transition region in one experiment very precisely.

4.2.2   *Specific heat properties*

As it has been found that for borosilicate and soda-lime-silicate glasses the volume and enthalpy relaxation kinetics are experimentally indistinguishable from one another [31-33, 35, 44], specific heat, c_p, measurements by differential scanning was investigated to understand the time and temperature dependence of glass properties through the transition region. First, the melting peak of zinc was measured in the experimental set-up of the DSC (for details see **Appendix B** and **C**) and the result is shown below for the zinc placed inside N-BK7 glass with a scanning rate of 4 K min^{-1}.
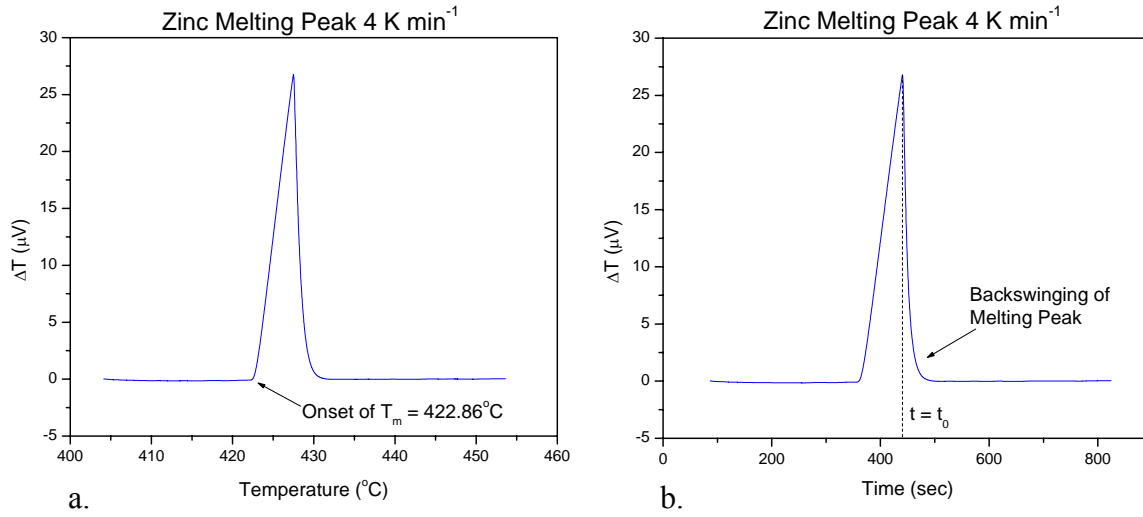
Fig. 4.9: Analysis of the zinc melting peak for the determination of the measured onset of T_m (a), and determination of the time constant τ_c of the backswinging of the melting peak (b).

The Fig. 4.9 shows the direct ΔT between the sample and reference pan monitored by the DSC at 4 K min^{-1} as a function of temperature (Fig. 4.9a) and time (Fig. 4.9b) for the zinc metal placed inside N-BK7 glass. The onset of the melting peak of the zinc was found to be 422.86^{o}C compared to the theoretical value of 419.53^{o}C. The difference between measured and theoretical values was used to apply a linear temperature correction to calibrate the sample temperature thermocouple. Fig. 4.9b shows that the ΔT signal after the zinc melting peak is "smeared", or delayed with time [53]. The time constant, τ_c, for this delay was determined from the zinc melting in Fig. 4.9b using the following simplified equation for the measured ΔT [32, 53]

$$-\Delta T(t) = C_1 + C_2 \cdot \exp\left(-\frac{t}{\tau_c}\right) = C_1 + \tau_c \cdot \Delta \dot{T}(t) \qquad (4.3)$$

where C_1 and C_2 are assumed constants, and $\Delta \dot{T}$ is the time derivative of the measured ΔT. By setting the time equal to zero, t_0, at the zinc melting peak, a first order exponential decay can be curve-fitted using equation (4.3) to find the τ_c, which was determined to be 9.00 s for the measurement shown in Fig. 4.9b. The temperature and τ_c calibration measurements of zinc metal placed inside N-BK7, P-SK57, and L-BAL35 glass samples were measured in the DSC at 4 and 8 K min^{-1} and the results are shown in the table below.

Table 4.5: Results for determining the onset of the T_m and the relaxation time constant, τ_c, of zinc for N-BK7, P-SK57, and L-BAL35 glasses at 4 and 8 K min^{-1}.

	N-BK7	P-SK57	L-BAL35
T_m (@ 4 K min^{-1}) ($^{\circ}$C)	422.86	422.92	422.77
T_m (@ 8 K min^{-1}) ($^{\circ}$C)	423.78	423.77	423.68
τ_c (@ 4 K min^{-1}) (s)	9.00	8.02	8.87
τ_c (@ 8 K min^{-1}) (s)	9.01	7.93	8.91

The calibration results shown in Table 4.5 provide the necessary results in order to *i)* calibrate the sample temperature thermocouple (for details see **Appendix B**) and *ii)* calibrate the ΔT between the glass sample and reference pan measured by the DSC (for details see **Appendix C**).

With the necessary thermocouple calibrations, equation (4.3) was revisited for the application of measuring a glass sample through the transition region, where the C_1 is no longer assumed constant. The derived equation explaining the measured ΔT with respect to sample heat capacity, C_s, is shown below

$$- \Delta T = R \cdot C_s \cdot \dot{T_o} + \tau_c \cdot \dot{\Delta T} \tag{4.4}$$

where R is the thermal resistance between the furnace and the platinum pan and $\dot{T_o}$ is the scanning rate (note that specific heat is defined as the heat capacity normalized to sample mass). Sapphire was measured as a sample with a known heat capacity which is not exposed to any state or phase transitions up to test temperatures for the glass of 650°C (sapphire $T_m = 2050$°C), and therefore the second term of equation (4.4) can be neglected and the R value can be determined. For a known R, and τ_c value, the heat capacity of an unknown glass sample can be determined from the ΔT signal from the DSC. Using equation (4.4), the determined c_p of the glass is no longer "smeared", or delayed with time, as the second term of the equation corrects [53]. The equation often used for c_p measurements that does not "de-smear" the results is given below [52]

$$c_{p,gl} = c_{p,st} \cdot \frac{\Delta T_{gl} \cdot m_{st}}{\Delta T_{st} \cdot m_{gl}} \tag{4.5}$$

where, $c_{p,gl}$ and $c_{p,st}$ is the specific heat of the glass and sapphire standard respectively, ΔT is the measured signal from the DSC, and m is the sample mass. The figure below shows the results for the c_p measurements made of N-BK7 glass at 4 and 8 K min^{-1} and the effects of "de-smearing" the measured ΔT from the DSC compared to previously determined data for BK-7 glass.
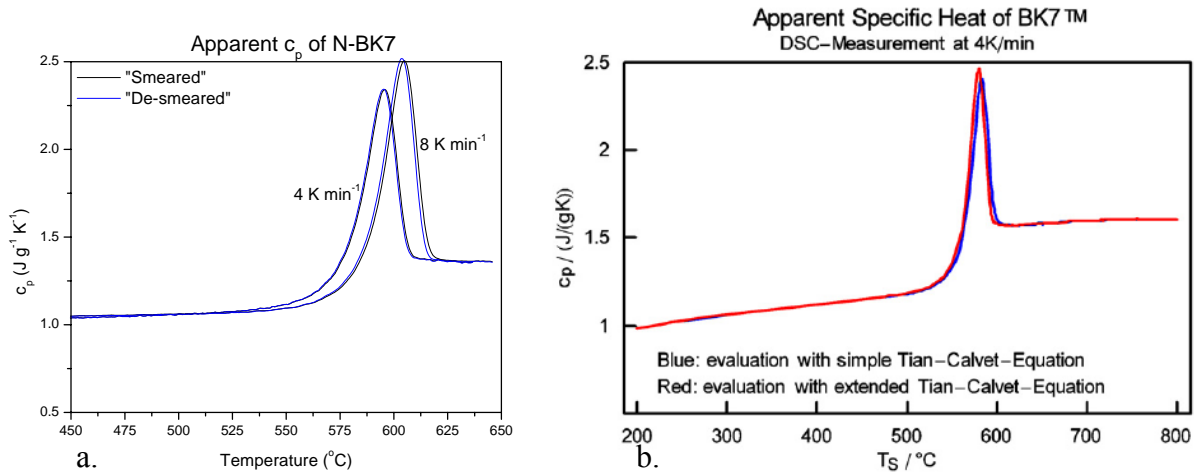
Fig. 4.10: Apparent specific heat of N-BK7 glass measured at 4 and 8 K min^{-1} according to equations (4.4 and 4.5) (a), and the apparent specific heat of BK-7 measured at 4 K min^{-1} from Fotheringham *et al* [32] (b).

Fig. 4.10a shows the c_p curve measured at two different heating rates through the glass transition region (approximately 540 – 625°C). The N-BK7 glass samples were annealed at 505°C for greater than 200 hours prior to the DSC scan to ensure that precise equilibration was allowed and that all samples had the exact same thermal history (details of DSC sample preparation are found in **Appendix D**). The specific heat in the glassy state, $c_{p,g}$, of N-BK7 was found to be (1.06 ± 0.53) J g^{-1} K^{-1} (at 495°C), and that the rate-dependent apparent specific heat begins to rise as it enters the transition region where the configurational response begins to contribute to the vibrational response of atoms. The specific heat in the liquid state after the glass transition region, $c_{p,l}$, of N-BK7 was found to be (1.36 ± 0.68) J g^{-1} K^{-1} (at 635°C). Fig. 4.10a also shows the effects of "de-smearing" the c_p curve. It can be seen that by not applying the technique of "de-smearing" the c_p measurements according to equation (4.4), the apparent c_p shifted too high by as much as 2°C. Fig. 4.10b shows the c_p of BK-7 measured by Fotheringham *et*

al [32] at a heating rate of 4 K min^{-1}. It can be seen that while the $c_{p,g}$ of BK-7 appears to be similar to that of N-BK7, the temperature position of the peak max is at a slightly lower temperature and the $c_{p,l}$ is greater for BK-7. It should be noted that the intensity of the peak cannot be directly compared since the thermal history of the BK-7 glass is not precisely known. Also shown in Fig. 4.10b is the similar peak shift of the c_p curve by "de-smearing", or "evaluation with extended Tian-Calvet-Equation". It is important to note that the "de-smearing" cannot be directly compared between our results on N-BK7 and those found by Fotheringham *et al* on BK-7 as the instrument used in our studies was different and therefore the determined relaxation time constant, τ_c, is also likely different. For more details on the differences between the disc-type heat flux DSC used for our measurements compared to the cylinder-type heat flux DSC used in the studies by Fotheringham *et al* see [59]. Although the temperature position of the transition measured in this study for N-BK7 and that measured of BK-7 by Fotheringham *et al* in [32] do not agree, we currently do not have sufficient information to conclude the two glass types are significantly different in composition. As Fotheringham *et al* used a different device for measurement in addition to a different temperature calibration (analysis of Aluminum melting peak for calibrations applied to measurements of BK-7 rather than zinc as was done for our study), the validity of these calibrations should be re-visited for the measurement of these glasses. The Zinc melting peak occurs at approximately 100°C below the transition range of N-BK7 and BK-7, while the Aluminum melting peak occurs approximately 100°C above the transition range of the two glass types. The application of these temperature and relaxation time constant

calibrations on both instruments should be re-visited with respect to their accuracy at different temperature ranges (specifically, the temperature range of the transition region measured for the glass).

N-BK7, P-SK57, and L-BAL35 glasses were annealed at 505, 445, and 480°C respectively for over 200 hours in order to ensure glass sample equilibration as was discussed for N-BK7 glass above. The technique of "de-smearing" the apparent c_p of the glasses upon measurements in the DSC at 4 and 8 K min^{-1} was employed and results are shown in the figure below.
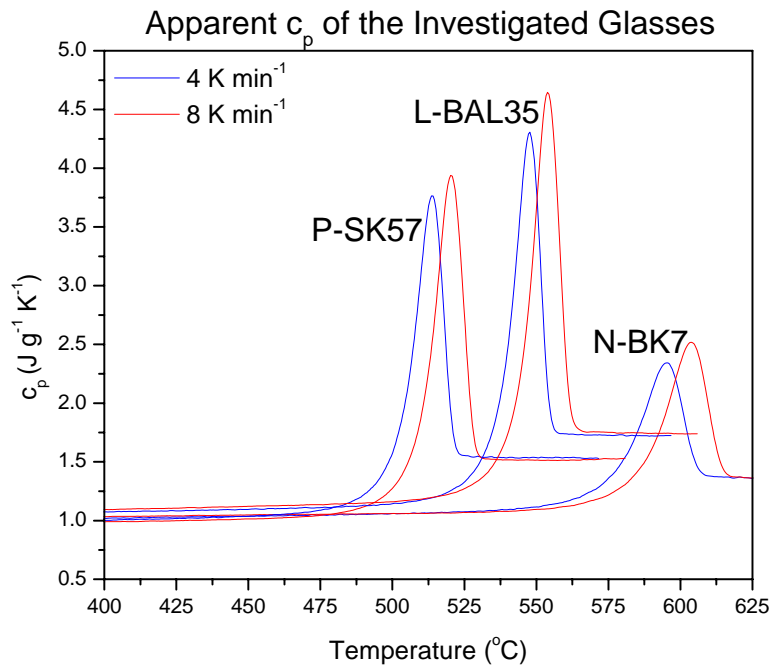
Fig. 4.11: Apparent c_p of N-BK7, P-SK57, and L-BAL35 glass types measured at 4 and 8 K min^{-1}.

Fig. 4.11 shows the results of the apparent c_p measurements of the temperature equilibrated glasses at 4 and 8 K min^{-1}. The position of the calorimetric glass transition

denoted by the peak of the apparent c_p curve of the investigated glass types relative to each other follows preceding observed trends that N-BK7 is a "higher-temperature" glass than P-SK57 and L-BAL35 (for viscosity, see Fig. 4.5, for thermal expansion, see Fig. 4.6). The c_p values of the glassy and liquid state (just above and just below the transition region, respectively) observed for the investigated glasses is seen below in Table 4.5.

Table 4.6: The c_p values of the glassy and liquid state of N-BK7, P-SK57, and L-BAL35 glasses determined from DSC measurements shown in Fig. 4.11.

	$c_{p,g}$ (J g^{-1} K^{-1})	$c_{p,l}$ (J g^{-1} K^{-1})	Δc_p (J g^{-1} K^{-1})
N-BK7	(1.06 ± 0.53) (at 495°C)	(1.36 ± 0.68) (at 635°C)	0.30 ± 0.02
P-SK57	(1.02 ± 0.51) (at 430°C)	(1.55 ± 0.78) (at 555°C)	0.53 ± 0.03
L-BAL35	(1.10 ± 0.55) (at 465°C)	(1.73 ± 0.87) (at 575°C)	0.63 ± 0.03

The measurements shown in Fig. 4.11 and the results given in Table 4.6 are similar to what was seen with respect to the thermal expansion coefficient values. In the glassy state, the α_g and $c_{p,g}$ values are very close between glass types; however, in the liquid state, α_l and $c_{p,l}$ for L-BAL35 were notably greater than those values for the other glass types, while for N-BK7 notably less. The Δc_p is shown in Table 4.6, again indicating the larger configurational contribution for L-BAL35 on top of the vibrational contribution (similar for all three glass types) after the step of the calorimetric glass transition (see also Table 4.4 for similar observations for thermal expansion).

Also noted from Fig. 4.11, L-BAL35 and P-SK57 exhibit similar calorimetric transitions of a very sharp and intense peak with L-BAL35 having a higher Δc_p. For similar peak intensities, it may not be unreasonable to think that the kinetics of the

configurational changes are similar for P-SK57 and L-BAL35. On the other hand, N-BK7 has a much less intense and broader peak than the other two glass types. The peak intensity of the calorimetric glass transition is a characteristic that depends upon the temperature at which the glass was equilibrated, where the lower the equilibration temperature of the glass, the more intense the calorimetric peak at the glass transition. However, N-BK7 was equilibrated at a temperature 66°C below the temperature corresponding to $10^{12.0}$ Pa s, whereas P-SK57 and L-BAL35 glasses were equilibrated at temperatures 39 and 48°C below the same viscosity point, respectively. Therefore, it may be deduced that the differing peak shape and intensity of the N-BK7 calorimetric glass transition from that of P-SK57 and L-BAL35 may have more to do with possible differing relaxation kinetics of the thermally activated atomic configurations.

4.3 Numerical Simulation Using the Tool-Narayanaswamy-Moynihan (TNM) Model

The TNM model was used to apply the above determinations of glass viscosity, thermal expansion, and specific heat information to behavior above, below, and within temperature ranges of the transition region. The TNM model was used to, first, model the kinetic response of determined c_p data, and second, apply those results to build a thermal expansion model. The precise c_p curves over the glass transition region were analyzed in order to determine the behavior of the fictive temperature, T_f, of the glass as a function of time and temperature upon heating according to equation (2.6). The first derivative of T_f with respect to temperature was used as experimental data to be curve-fitted to the TNM model in order to find the four structural relaxation parameters E/R, x,

β, and τ₀ using equations (2.13-2.18). It should be noted here that with respect to the study of the glass transition region, the activation energy, E, is in fact the activation energy for the glass transition (which is experimentally indistinguishable from the activation energy for viscous flow, E_η [56]). Finally, thermal expansion properties determined in section 4.2.1 in conjunction with the four determined structural relaxation parameters defining the first derivative of T_f with respect to temperature were used to develop a dynamic thermal expansion model according to equation (2.4).

Equation (2.6) was used in order to find the T_f as a function of temperature through the glass transition region. Boundary conditions for the upper temperature point at $c_{p,l}$ were chosen to be at a temperature just above the transition region where it can be assumed $T_f = T$. The lower temperature point at $c_{p,g}$ was determined to be just below the transition region where it can be assumed that T_f does not change with changing T. The upper and lower-bound points were also chosen so that the range of temperatures for the integration of the cp was as narrow as possible ensuring the valid assumption of constant activation energy across the temperature region of interest. The $c_{p,g}$ value was chosen to be a temperature approximately $10 - 20^{\circ}C$ below the temperature at which the glass samples were equilibrated, and the $c_{p,l}$ value was chosen to be approximately $10 - 20^{\circ}C$ above the transition peak (see Table 4.5 for glass type details). Using equation (2.6), the T_f as a function of temperature and its first derivative were determined from the c_p curve shown in Fig. 4.11 of N-BK7 glass and is shown below.
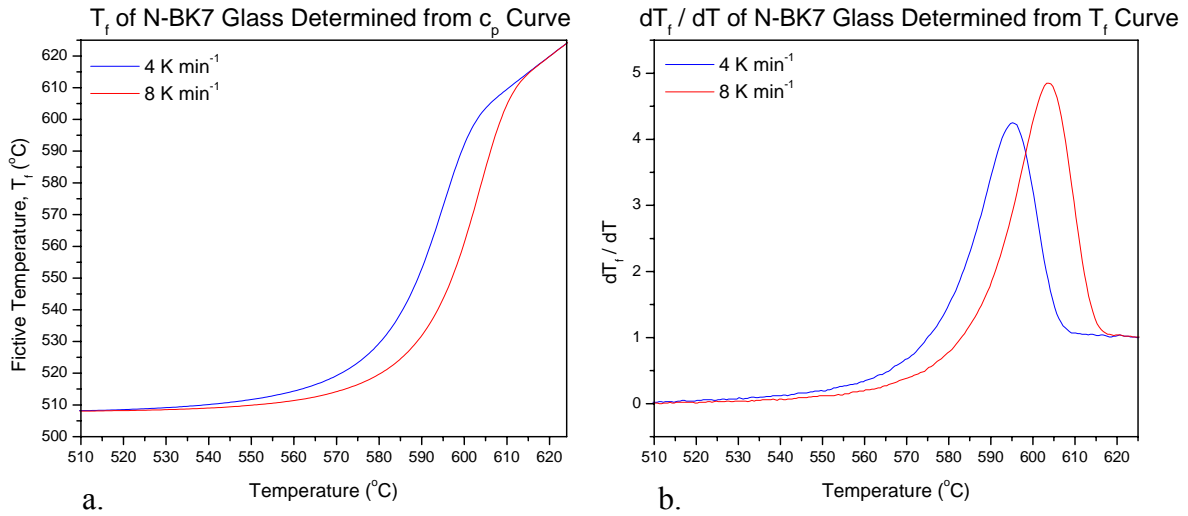
Fig. 4.12: Fictive temperature (a) and its first derivative (b) as a function of temperature upon heating at 4 and 8 K min^{-1} determined from the c_p curve.

Fig. 4.12 shows the result of integrating the c_p curve of N-BK7 glass using equation (2.6) in order to find the T_f as a function of temperature (Fig. 4.12a). The result shows that at low temperatures, the initial T_f value, $T_{f,0}$, was 508°C which corresponds to the 505°C at which the glass was equilibrated. This indicates that, within the expected error of the thermocouples monitoring the 200-hour equilibration and the thermocouples of the DSC, the sample was sufficiently equilibrated. If the determined $T_{f,0}$ was *higher* than the equilibration temperature, we would determine that either not enough time was allowed for equilibration, or the temperature was too low. However, if the determined $T_{f,0}$ was *lower* than the equilibration temperature, we would determine that the equilibration temperature was too high, and therefore some relaxation of the glass sample occurred upon removing it from our furnace. For this reason there is a discrepancy between the relationship of the equilibration temperature with the $T_{12.0}$ value (66°C, 39°C, and 48°C

below $T_{12.0}$ for N-BK7, L-BAL35, and P-SK57 respectively). We could not choose a temperature of equilibration value that corresponded to a specific viscosity as it is not reasonable to discuss viscosity behavior well below the annealing region, and thus the temperature difference below the $T_{12.0}$ depends upon structural relaxation processes different for each glass type. Therefore, the magnitude of the equilibration temperature below the $T_{12.0}$ value was validated by determining the calculated $T_{f,0}$ value from c_p measurements was the same as the temperature of equilibration.

Thus, in this way the experimental finding of $T_{f,0}$ corresponding to the equilibration temperature also confirms that all the fictive "sub" temperatures, $T_{f,i}$, are equivalent and also correspond to the equilibration temperature of the glass sample. In fact, for all investigated glass types, the results of the integration of the c_p curve (T_f as a function of T) ensured that the $T_{f,0}$ values matched the temperature of glass equilibration. As the glass heats into the glass transition region, the T_f begins to increase from $T_{f,0}$ and it can be seen that this occurs at lower temperatures for the lower heating rate because there is more time allowed for the slow, thermally activated atomic configurational relaxation kinetics. Fig. 4.12b further confirms the sole vibrational contribution to the material response at low temperatures where the change in T_f with respect to temperature is zero. As sufficient thermal energy is reached in the glass transition region, the change in T_f with respect to the change in temperature increases to a maximum (intensity of which is dependent upon cooling and reheating rates) before reaching the super-cooled liquid state where the atomic configurational changes become instantaneous with changes in temperature ($dT_f / dT = 1$).

With the experimentally determined data for the changes of the equilibrium temperature of the glass, T_f, with respect to changes in temperature, a curve-fitting routine was performed to find the E/R, x, β, and τ_0 values defining the structural relaxation kinetics of the glass transition region. Before sharing details of the routine, a brief explanation of the effects of the four parameters on the relaxation kinetics is necessary. The temperature position of the peak is dictated largely by the activation energy for the glass transition, E (assumed constant over the narrow range of temperatures), and the relaxation time constant, τ_0. For a fixed value of E/R, increasing values of τ_0 shift the transition peak to higher temperatures, and the same holds true for fixed values of τ_0 and increasing values of E/R. The peak shape and intensity is mostly attributed to the non-linearity parameter, x, and the non-exponentiality parameter, β (both ranging in value between 0 and 1). As may be expected from their assigned name, the two values are inversely related so that a decrease in x, or an increase in β, the transition peak narrows and increases in intensity and visa versa.

The concepts described above for the contribution of each of the four TNM model parameters was used to determine a working curve-fitting technique similar to that which was performed by Fotheringham [35]. First, the activation energy for viscous flow, E_η, was taken as the initial guess value for E of the TNM model, as it has been previously shown that it is in fact reasonable to assume the activation energy for viscous flow and the glass transition are close in value [56]. The initial guess of E was used to compute the E/R value (units of K), and, in turn, to compute the initial estimate of the τ_0 (units of s) according to [35]

$$\dot{T} \cdot \tau_0 \cdot e^{\left(\frac{E}{R \cdot T_{\text{infl}}}\right)} \approx 1, \qquad\qquad\qquad\qquad (4.6)$$

where T_{infl} is the inflection point of the lower heating rate, $\dot{T}$, curve. The initial guess values for x and β were both assumed to be 0.75. With starting values of E/R, x, β, and τ_0, an optimization routine was performed to curve-fit the experimental dT_f / dT data (4 and 8 K min^{-1}) for N-BK7, P-SK57, and L-BAL35. Without data measured at two different heating rates, we would not be able to determine a working solution due to the mathematical complexity of the TNM model.

It was found that four separate loops for computing the relaxation parameters were necessary to obtain a realistic and best-fit solution. In the first loop, E/R, x, and β values were held constant while the τ_0 value was changed so that the inflection point between the theoretical and experimental curves of the lower heating rate curve coincided. In the second loop, x and β were held constant and E/R and τ_0 values were optimized such that the conditions of the first loop remain, and in addition, the inflection points of both the theoretical and experimental curves of the higher heating rate were the same. In the third loop, all values were allowed to change such that the conditions of the preceding two loops were met, and in addition, the temperature position of the peak max for the theoretical and experimental curves were the same in the case of the lower and higher heating rate curves. In the fourth loop, all parameters were changed so that the difference was minimized between the theoretical and experimental curves of both heating rates for the five highest data points (the five largest dT_f / dT values) of each peak. Although the path from initial guesses to the conditions of the third loop were different, Fotheringham

found that the conditions of the third loop were sufficient to converge to a solution [31]. However, by incorporating the conditions of the fourth loop explained here, the four structural relaxation parameters are optimized not only with respect to the temperature (x-axis) position (first three loops) of the curve but also the dT_f / dT (y-axis) position (fourth loop). Seen below are the results of the curve-fitting for N-BK7, P-SK57, and L-BAL35 glass types.
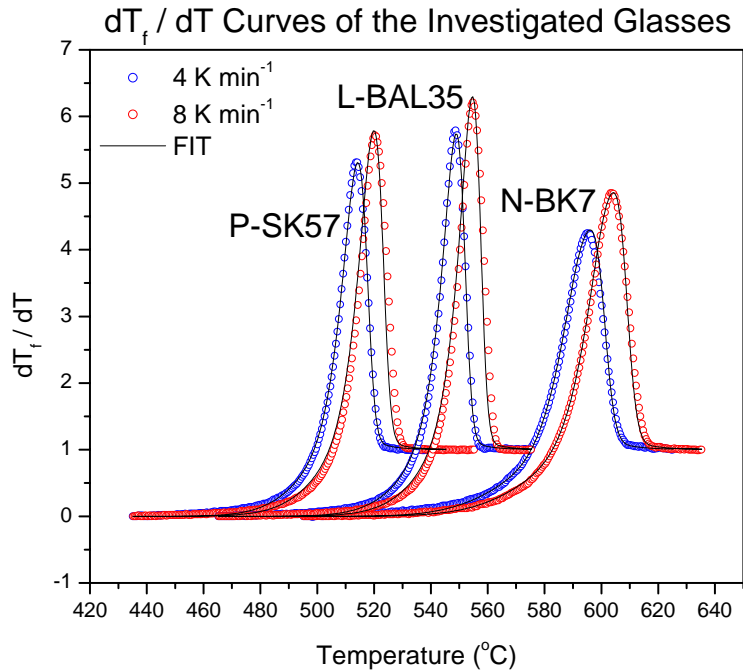
Fig. 4.13: Curves from differential scanning calorimetry experiments curve-fitted to the TNM model parameters.

Fig. 4.13 shows that a good curve-fit of the dT_f / dT curves for the investigated glasses was determined, resulting in the values for the four structural relaxation parameters that converge to a working solution. The determined structural relaxation parameters were

$E/R = (72,782 \pm 3639)$ K, $x = 0.702 \pm 0.035$, $\beta = 0.706 \pm 0.035$, $\tau_0 = (9.62 \pm 0.48) \times 10^{-36}$

s for N-BK7, $E/R = (82,245 \pm 4112)$ K, $x = 0.752 \pm 0.038$, $\beta = 0.774 \pm 0.39$, $\tau_0 = (8.19 \pm 0.41) \times 10^{-45}$ s for P-SK57, and $E/R = (90,608 \pm 4530)$ K, $x = 0.745 \pm 0.037$, $\beta = 0.802 \pm 0.040$, $\tau_0 = (2.44 \pm 0.12) \times 10^{-47}$ s for L-BAL35. Similar values were found for P-SK57 [44] where the $E/R = 84,396$ K, $x = 0.789$, $\beta = 0.656$, $\tau_0 = 1.68 \times 10^{-46}$ s. It is unknown why the τ_0 value determined from our measurements above and which was determined in [44] are different, but as mentioned before, the temperature calibrations performed in our laboratory and that performed by Fotheringham *et al* were different. It may be that both methods of temperature calibration should be revisited before determining a more precise τ_0 value. However, the other three parameters are seem to be in agreement with those found by Fotheringham *et al*, possibly confirming that the techniques used for modeling the kinetics of the transition region could be repeated.

The activation energy for the glass transition, E, normalized to the ideal gas constant, R determined from the DSC measurements do not appear to agree with the E_η/R value with the exception of those determined for N-BK7. The E/R value shown above for P-SK57 and L-BAL35 was considerably lower than the E_η/R value determined from viscosity measurements. It is likely due to the fact that a very extensive temperature calibration was performed for DSC measurements, and no such calibration was considered for the beam-bending or parallel-plate viscometers. As a result, the level of accuracy of the viscosity measurements may be less than that which we obtained from DSC measurements. It is expected that the determined TNM model parameters from the DSC measurements shown above may be used to model the kinetics of glass property behavior through the glass transition region – specifically the thermal expansion.

In order to apply the structural relaxation findings to a working thermal expansion model that can be universally applied to various cooling profiles of the molding process, various inputs must be specified. The inputs for this model are, *i)* the molding temperature, *ii)* the α_g, *iii)* the α_l, and *iv)* the four structural relaxation parameters to the TNM model, and their values are shown below in Table 4.7

Table 4.7: Material inputs to a thermal expansion model for the cooling profile from the molding temperature.

	N-BK7	P-SK57	L-BAL35
$T_{molding}$ $(10^{8.0}$ Pa s) $\pm 10^{o}C$	671	554	587
$\alpha_g \pm 0.1 \times 10^{-6}$	8.2×10^{-6} /K	9.2×10^{-6} /K	8.2×10^{-6} /K
$\alpha_l \pm 1 \times 10^{-6}$	54×10^{-6} /K	62×10^{-6} /K	70×10^{-6} /K
E/R $\pm 5\%$	71,704 K	82,245 K	90,608 K
x $\pm 5\%$	0.708	0.752	0.745
$\beta \pm 5\%$	0.721	0.774	0.802
$\tau_0 \pm 5\%$	3.56×10^{-36} s	8.19×10^{-45} s	2.44×10^{-47} s

The $T_{molding}$ shown above in Table 4.7 was chosen to be the lower-bound temperature appropriate for molding which corresponds to a Log viscosity of 8.0 Pa s. As indicated by the viscosity curve in Fig. 4.5, N-BK7 glass is a higher temperature glass than the P-SK57 and L-BAL35 re-affirming the result displayed in Table 4.7 that it does have a higher temperature appropriate for molding. This means that there is a larger temperature range for which it is cooled and may initially lead one to think that N-BK7 may exhibit more thermal contraction according to some α than the other two glass types. On the contrary, P-SK57 has the lowest $T_{molding}$ indicating there is a smaller temperature range for thermal contraction to occur according to some α, and therefore, may exhibit less

thermal contraction than the other two glass types. However, N-BK7 has a α_l value lower than both P-SK57 and L-BAL35 meaning that N-BK7 would be expected to contract less upon cooling at higher temperatures than the other two glass types. Accordingly, L-BAL35 has the largest al value at (7.0 ± 1) x $10^{-6}\,K^{-1}$ indicating that this glass contracts most in the higher temperature region than the other two glasses. Furthermore, the four structural relaxation parameters are shown as the material constants defining the kinetics at which the α_l value transitions to the α_g value when cooled from the $T_{molding}$. As mentioned before, the E/R and τ_0 values control largely the position of the transition region in such a way that an increase in E/R has a similar effect as a decrease in τ_0, and β and x values have a similar relationship but are discussed with respect to their influence on the rate of relaxations within the transition region. Therefore, as one might imagine, it is difficult to discern how the results for the structural relaxation parameters may translate to effects on the kinetics through the transition region. For this reason, a computation of the thermal expansion behavior incorporating all data in Table 4.7 was performed. A realistic cooling rate from the $T_{molding}$ value was chosen as 30 K min^{-1} to show how the thermal expansion of each glass type may behave as a function of its α_g, α_l, and structural relaxation values. The thermal expansion model computed from equation (2.4a) for N-BK7, P-SK57, and L-BAL35 glass types upon cooling from $T_{molding}$ is shown in Fig. 4.14.
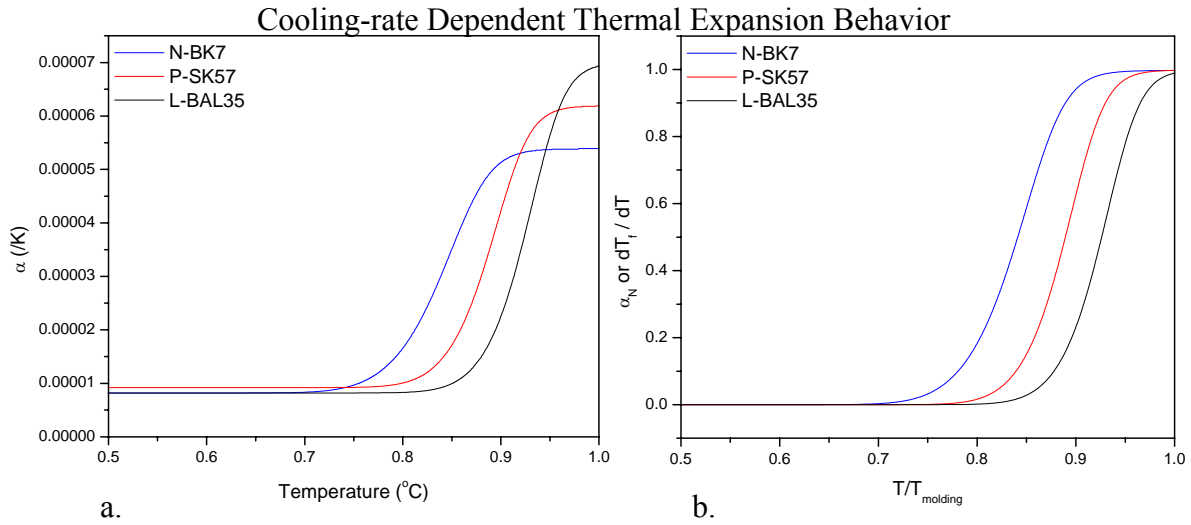
Fig. 4.14: Calculated thermal expansion (a) and normalized thermal expansion (or dT_f / dT) (b) upon cooling from the $T_{molding}$ for N-BK7, P-SK57, and L-BAL35 glass types using the inputs from Table 4.6.

The figure shows the application of the TNM model to predict the behavior of the thermal expansion coefficient upon cooling at 30 K min^{-1} from a molding temperature determined to be at a viscosity of $10^{8.0}$ Pa s. Fig. 4.14a shows the actual thermal expansion coefficient upon cooling reflecting the notably different α_l values between all three glasses, yet similar α_g values. It shows that for P-SK57 and L-BAL35, the $\alpha(T)$ begins to change very rapidly, and over a very short range of temperatures, the α_l transitions to the α_g value. On the other hand, while N-BK7 does have a lower α_l than P-SK57 and L-BAL35, the temperature range in which it transitions to the α_g value is larger, indicating that more thermal shrinkage may occur than for the other two glasses with the same cooling profile. In fact, at 25°C, the calculated total relative linear thermal shrinkage upon cooling from $T_{molding}$ at 30 K min^{-1} was 10.3 x 10^{-3} for N-BK7, 8.2 x 10^{-3}

for P-SK57, and 7.4 x 10^{-3} for L-BAL35. This indication is further confirmed by observing the normalized thermal expansion (α_N) or dT_f / dT plot upon cooling. Fig. 4.14b shows the α_N plotted as a function of $T/T_{molding}$ and it can be seen that when the thermal expansion is normalized to their respective coefficients of the glassy and liquid state, N-BK7 glass does in fact shrink much more upon cooling than P-SK57 or L-BAL35.

This observation of N-BK7 shrinking more than the other glasses when cooled from the same viscosity value indicates that it is not necessarily the value of the thermal expansion of the liquid that dictates overall glass shrinkage on cooling, but rather, the temperature and time-scale at which the configurational changes in the glass occur. Without the incorporation of structural relaxation, it would not be possible to model the kinetics at which the α_l value transitions to the α_g value, and therefore, we would not have been able to accurately define such a thermal expansion model as shown in Fig. 4.14.

Previously in Fig. 4.5 and 4.6, it was shown that N-BK7 glass is a more 'strong' glass than P-SK57 and L-BAL35 with equal changes in viscosity requiring greater changes in temperature. Viscosity is a *stress* relaxation characterization rather than *structural*; however, the viscosity does depend upon temperature making it a property whose time and temperature-dependent behavior is connected to structural relaxation mechanisms. Therefore, it is reasonable to think that the configurational changes within the glass are closely liked to the allowable kinetics for viscous flow. This may especially be assumed over the limited range of temperatures for which the activation energy (for the glass

transition region or viscous flow) can be assumed constant. Therefore, for the glass types discussed within this study, a relationship may be drawn between kinetic fragility, m, of the glass and the degree to which the glass may be expected to shrink upon cooling modeled by the TNM parameters. N-BK7 had the lowest fragility of the investigated glasses (m = 39) and the most normalized thermal shrinkage when cooled from the same viscosity value. On the other hand, L-BAL35 had the highest fragility (m = 59) and the lowest normalized thermal shrinkage.

CHAPTER FIVE

CONCLUSIONS

A systematic series of experimental and computational methods defining material property parameters and their use in a predictive model of the PGM process have been established. Through interdepartmental collaboration at Clemson University and industrial support from Edmund Optics and the U.S. Army at Benét Laboratories, the molding process was defined from a mechanical and material perspective. The key findings generated by the team addressed heat-transfer, pressure, temperature, and time effects on both mold and glass materials throughout the molding process.

The characterization of glass properties, which was the focus of this thesis, consisted of defining the viscosity, thermal expansion, and structural relaxation properties needed for implementation into a predictive model of material behavior. The viscosity was measured to define appropriate temperatures for molding. Thermal expansion and structural relaxation processes were quantified in multiple glass types to define a thermal expansion model precisely predicting glass expansion and contraction upon exposure to the PGM process (heating and cooling). Viscosity, thermal expansion, and structural relaxation measurement protocols were developed using commercial optical glasses N-BK7 and P-SK57 glasses of SCHOTT and data was compared to previously found values (either through literature or private communication). The viscosity and expansion properties of a moldable, L-BAL35 glass of OHARA were determined to demonstrate the implementation of the method.

Beam-bending and parallel-plate techniques were used to measure the viscosity of the investigated glass types to define an appropriate temperature range for molding. Our measurements showed:

- Through viscosity measurements, the molding region was $664 - 732^{\circ}$C for N-BK7, $549 - 598^{\circ}$C for P-SK57, and $583 - 628^{\circ}$C for L-BAL35.

- The broader molding temperature range of N-BK7 was explained due to its more 'strong' viscosity curve quantified by its low kinetic fragility parameter (m = 39).

- Thermal mechanical analysis (TMA) measurements were used to determine the α_g and α_l of the investigated glass types. Rate-heating thermal expansion measurements were found sufficient to specifically determine expansive properties in the glassy state, but isothermal measurements in the glass transition region were employed to estimate the α_l.

- Transient expansion behavior in the glass transition region was estimated by precisely measuring transient enthalpy behavior quantified by the c_p. The c_p measurements were used to curve-fit the well-known TNM structural relaxation model for the kinetic response of glass in the glass transition region.

- Structural relaxation parameters were found for the glasses of interest through the use of a newly developed optimizing curve fitting procedure. Incorporating experimentally determined data into the optimization routine, the four parameters of interest for our three glass types were determined to be:

    - $E/R = (72,782 \pm 3639)$ K, $x = 0.702 \pm 0.035$, $\beta = 0.706 \pm 0.035$, $\tau_0 = (9.62 \pm 0.48) \times 10^{-36}$ s for N-BK7

- $E/R = (82,245 \pm 4112)$ K, $x = 0.752 \pm 0.038$, $\beta = 0.774 \pm 0.39$, $\tau_0 = (8.19 \pm 0.41) \times 10^{-45}$ s for P-SK57

and

- $E/R = (90,608 \pm 4530)$ K, $x = 0.745 \pm 0.037$, $\beta = 0.802 \pm 0.040$, $\tau_0 = (2.44 \pm 0.12) \times 10^{-47}$ s for L-BAL35.

Lastly, a compiled thermal expansion model was constructed to show the thermal expansion coefficient upon cooling at a known rate from the molding temperature. We were able to show the importance of obtaining not only the α_g and α_l properties, but also the rate-dependent response of the thermal expansion defined by structural relaxation. The thermal expansion model showed:

- When molding at the same viscosity and cooling at the same rate, more thermal shrinkage was noted for N-BK7 than for P-SK57 or L-BAL35.

- Without the incorporation of the structural relaxation effects, the rate-dependence would not have been possible. Through the determination of the rheological and thermal expansion properties and the structural relaxation parameters, we have

  - defined a method for determining viscosity and thermal expansion behavior of glass within the molding region of temperatures

  - developed a thermal expansion model that can be applied to the molding process with any imposed cooling rate

  - quantified thermal shrinkage of glass upon cooling from the molding temperature by directly computing the thermal expansion coefficient as a function of temperature with the thermal expansion model.

The results and developed methods within this thesis will extend future researchers' ability to characterize glass properties of additional moldable glass types in order to precisely predict behavior through the PGM process. To reach these goals, the methods for glass material characterization that have been developed may yield findings not previously realized. The challenge will be to show how the suite of tools discussed within this thesis strengthens the foundation for improving the manner in which one makes lens molding a cost-efficient method for providing aspherical lenses to the optical industry. Moldable glass types vary greatly in glass composition and structure, and so the viscosity, thermal expansion, and specific kinetics of structural relaxation properties studied for their relationship to glass structural attributes would greatly benefit the glass molding industry. Now that the method for structural relaxation characterization has been developed in this study, the relaxation of other glass properties, such as refractive index, can be performed validating the universality of the TNM model and thus predicting optical quality of molded lenses. Implementation of viscosity, thermal expansion, and structural relaxation properties to a finite element model can be used to determine the sensitivity of modeling results with respect to the material property inputs, which further contributes to the study of the macroscopic application of the TNM model. The compiled finite element model not only will allow predictions of final shape and size of the lens, but it will also facilitate the necessary reverse engineering for designing the required mold shape.

APPENDICES

A. Solution to Tool's Original Differential Equation for the Fictive Temperature

The original differential equation for the change in T_f with respect to time is given below

$$\frac{dT_f(t)}{dt} = \left(\frac{1}{\tau}\right) \cdot T(t) - \left(\frac{1}{\tau}\right) \cdot T_f(t) \tag{A.1}$$

where the relaxation time τ is defined as

$$\tau = \tau_0 e^{\frac{E}{RT}} \tag{A.2}$$

where τ_0 is the relaxation time constant and E/R is the activation energy. The equation (A.1) takes the form of a heterogeneous differential equation. The solution to a heterogeneous differential equation takes the form of a general solution to the homogeneous equation and a particular solution to the heterogeneous equation. The initial approach for the formula for T_f is the following giving the general solution to a homogeneous equation

$$T_f = C \cdot e^{-\frac{t}{\tau}} \tag{A.3}$$

where C is a constant. The time derivative of equation (A.3) is the following

$$\frac{dT_f(t)}{dt} = e^{-\frac{t}{\tau}} \cdot \left[-\frac{1}{\tau} \cdot C + \dot{C} \right] \tag{A.4}$$

where $\dot{C}$ is the derivative of *C*. Inserting equation (A.3) into equation (A.1) and setting equal to equation (A.4), one finds the equation for $\dot{C}$ to be the following

$$\dot{C} = \frac{1}{\tau} \cdot T \cdot e^{\frac{t}{\tau}} \tag{A.5}$$

and the solution for C is determined by integrating equation (A.5)

$$C = \int \overset{\bullet}{C} \cdot dt = \frac{1}{\tau} \cdot T \cdot \int e^{\frac{t}{\tau}} \cdot dt$$
$$= T \cdot e^{\frac{t}{\tau}} + D$$

(A.6)

where D is the constant obtained from the integration. By inserting the solution to equation (A.6) into equation (A.3), one finds an equation for T_f

$$T_f(t) = \left(T \cdot e^{\frac{t}{\tau}} + D \right) \cdot e^{-\frac{t}{\tau}}.$$

(A.7)

For an isothermal case, a boundary condition can be applied that shows when t=0, T_f=T, and therefore, $D=T_f(0)-T$. Inserting this value for D into equation (A.7), one finds the following solution to Tool's original differential equation (A.1)

$$T_f(t) = T + (T_f(0) - T) \cdot e^{\frac{-t}{\tau}}$$

(A.8)

where now the equation (A.8) is equivalent to equation (2.8) in the text.

B. Sample Temperature Thermocouple Calibration of the DSC 2920 of TA Instruments

Below is the procedure for performing the temperature calibration for *each* glass type and *each* heating rate in the DSC.

1. Prepare glass disks of the glass types that are being investigated. They should be small enough in diameter to fit inside the platinum pans for the DSC (approximately 5.75 mm in diameter is sufficient). These disks should have parallel surfaces so that one surface is polished and the other is fine-ground. Thickness should be approximately 1 mm.

2. On the surface of the disk that is fine ground, drill a small hole in the top with a 1.10 mm diameter drill bit. The hole should be at least 0.5 mm deep.

3. Cut a small piece of zinc wire (99.999% pure of Goodfellow and 1 mm diameter), and place into the small hole at the top of the glass sample. A mass of approximately 1 – 3 mg is sufficient. Record the mass of the zinc.

4. Place the glass sample with the zinc wire inside the top hole into the platinum pan. This should be done so that the polished surface to the glass disk is in contact with the bottom of the platinum pan. Be sure to first measure the mass of the zinc.

5. It is important to note that the calibration should be done in platinum sample pans and a new platinum sample pan should be used when changing glass types.

6. Enter the TA Instruments software and ensure that you are in **calibration mode**.

    a. Under the Summary Tab

        i. Select zinc for the sample name

ii. The mass of the zinc can be entered, or simply recorded and later applied to the data "manually" by the user. Recording the mass for later application is recommended

iii. Select location for the placement of the file

iv. Select "Temperature" as the test procedure

b. Under the Procedure Tab

i. Start temperature should be $395^{\circ}C$

ii. Heating rate should be entered as the rate that will be used for measurements of the glass (4 and 8 K min^{-1} were the only rates used for this study)

iii. Max temperature should be $450^{\circ}C$

7. Once the glass/zinc sample is loaded into the DSC cell (step 4) and the TA Instruments software is set up (Step 5) click "Apply" in the TA Instruments software window. Ensure that the procedure specified in 5.b is displayed on the right side of the screen directly above the "Heat Flow versus Temperature" graph. If all changes and adjustments made were applied by clicking the "Apply" button, the "play" symbol will be displayed green.

8. Click the green "play" symbol to start the method.

9. When the method is complete, open the Universal Analysis software.

a. Open the specific calibration file of interest

b. At the bottom of the "Data File Information" window, click Exotherm "Up"

c. Click the "Signals" button

d. Under "Y1" select "Delta T (µV/mg)"

e. Under "Y2" select "Not Used"

f. Ensure that "Temperature (^{o}C)" is selected as "X" (This is default)

g. Click "OK"

h. Click "OK" again

i. If the user did not enter the mass (it was specified as "0.000 mg") for the experiment, when following through with step 8.h, a warning label will say "Cannot use normalized units with zero mass". This is OK as the user does not need the data normalized for mass for the temperature calibration. If the user wishes to normalize the "Delta T" signal for mass, this can be done manually, or by entering the mass in the box provided in the "Data File Information" window.

The file should look something like the data seen below where the melting peak of zinc was measured on a BK-7 glass disk sample at a heating rate of 8 K min^{-1}.
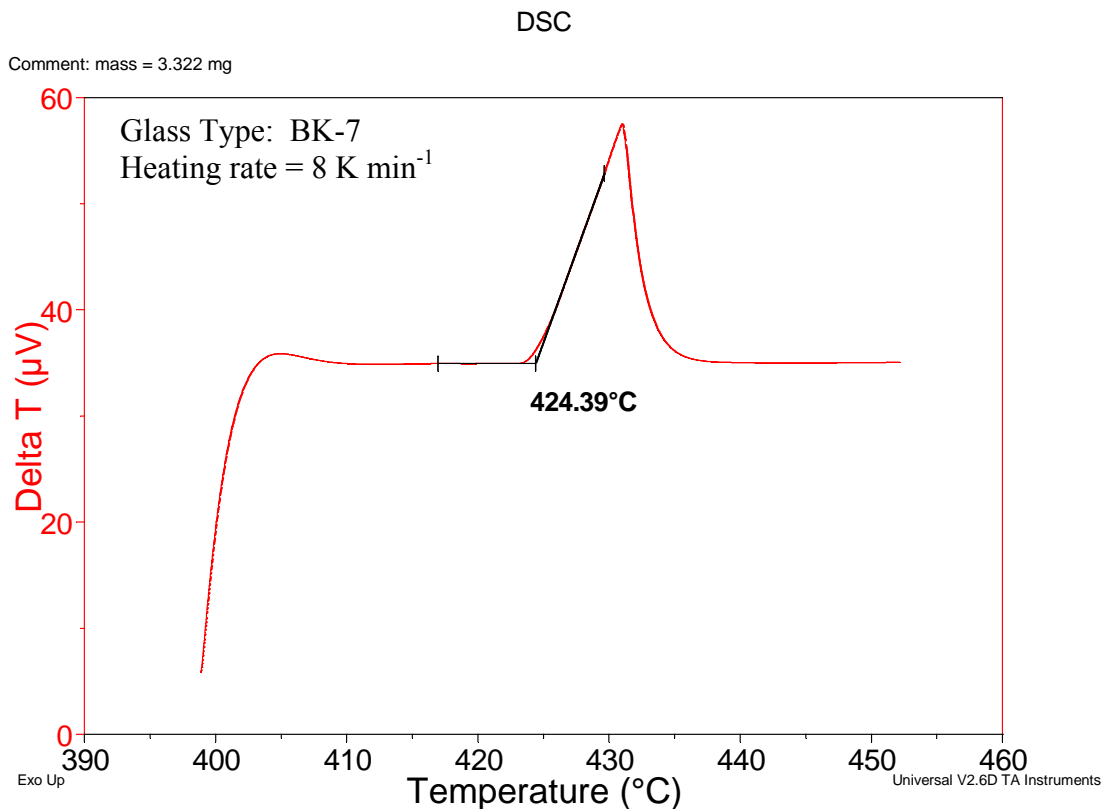
Fig. A.1: Melting peak of zinc measured at 8 K min^{-1} on a BK-7 glass disk sample.

The observed onset of the melting peak of zinc (T_s') measured at 8 K min^{-1} is shown above to be 424.39^{o}C and was computed in the following way:

1. When the data file is opened in the Universal Analysis software, right-click in the background of the data file

2. Select "Onset Point"

3. Four locations on the curve above need to be specified by either double-clicking on the curve, or dragging the point across the data shown above to the location desired:

a. The first two points should be before the onset of the melting peak. This gives a linear slope of the data between two points before the onset. In the case above, the two points were indicated on the data at approximately 416 and 420°C.

b. The second two points should be after the onset point along the increasing slope to the maximum of the melting peak. In the case above, the two points were indicated on the data at approximately 427 and 429°C

C. *Determination of the Time Constant τ_c*

No new measurements need to be made for the determination of the τ_c. The τ_c is determined from analyzing the melting peak measurements of zinc which was explained in detail in **Appendix B** above. It must be noted here, that the τ_c values need to be computed for **each** glass-zinc combination and **each** heating rate.

1. Open the first glass-zinc run at the specified heating rate in Universal Analysis

2. In the "Data File Information" window, click "Signals"

3. For Y1, select "Delta T (μV/mg).

4. For Y2, select "Not Used".

5. For X, select "Time".

6. Click "OK".

7. Select "Units" from the "Data File Information" window.

8. Under "General", select "sec' for "Time".

9. Click "OK"

10. Because the mass of the zinc was recorded and not inserted into the software, the error message will pop up saying "Cannot use normalized units with zero mass". Click "OK".

11. Click "OK".

12. At the bottom of the "Data File Information" window, select Exotherm: "Up".

13. Click "OK".

14. Now that the data file is opened, the user needs to find the time position of the peak max of the melting peak.

a. Right-Click in the background

b. Select "Peak Max".

c. Move the cross-arrows so that the peak max lies between the two. This can be done by double-clicking or dragging and dropping.

d. Right-Click and select "Accept Limits"

The following figure of the melting peak of zinc is shown below with the peak max indicated.

DSC

Comment: mass of glass = 68.491 mg AND mass of zinc = 4.857 mg
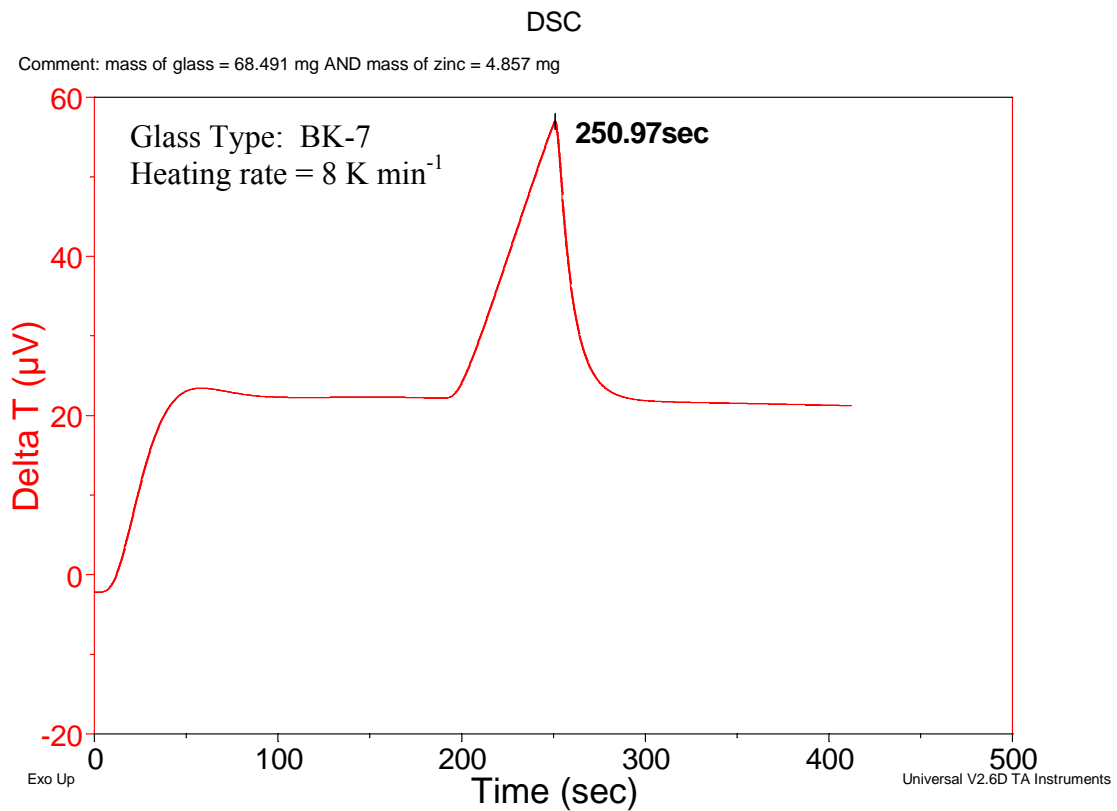
Figure A.2: Melting peak of zinc plotted as a function of time.

The figure above shows the complete time function of the "backswinging" of the ΔT signal of the melting peak of zinc. The time of the peak max is indicated really serves no other purpose than to indicate a starting position for extracting the data described below.

15. At the top of the screen, select the "Data File" under the "View" drop-down command.

16. Enter the time position of the peak max as the start position.

17. Enter a time that extends to the end of the data as the end position.

18. Click "all data points".

19. Click "OK".

20. Save the text file.

21. Import into excel on personal computer.

22. Plot the Delta T (μV) **versus** time (sec) in Origin

23. Subtract all time data points by the time position of the peak max. This makes the first time data point 0.

24. Plot the curve

25. Apply a first order exponential decay non-linear fit of the formulation:

$$y = y_0 + A_1 \cdot e^{-\frac{t}{t_1}} \hspace{3cm} \text{(C.1)}$$

where y_0 and A_1 are constants, y is the Delta T (μV) from the DSC, t is the time and t_1 is the time constant of the measurement τ_c. Use the non-linear fit to solve for τ_c as shown in the graph below.

Figure A.3: Measured and curve-fit backswinging of the melting peak of zinc placed on BK-7 glass measured at a scanning rate of 8 K min^{-1}.
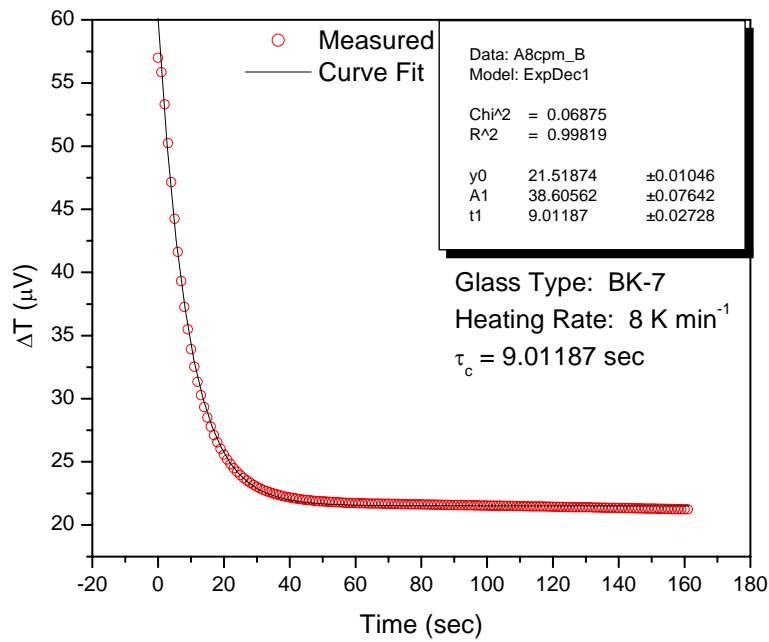
The figure shows the measured data points with the peak max data point being at time = 0 sec. The applied non-linear curve-fit according to equation (C.1) was used to find the τ_c value

D. Calculation of the specific heat of the glass sample, $c_{p,gl}$

Below is the procedure for performing the necessary runs and calculations to be done for calculating the c_p of a glass at a specific heating rate. Note that all runs 1-3 should be done with the reference pan empty. Each run heats from room temperature to a maximum temperature with isothermal holds at 100°C and the maximum temperature for 5 minutes. The maximum temperature should be chosen carefully depending on glass type. It must be high enough that the entire transition region is measured, but must remain below the maximum operating temperature of 720°C of the DSC and below temperatures at which the glass might begin reacting with the crucible. If this maximum temperature is not initially known, a "dirty" crucible should be used to make a single scan to an estimated maximum temperature (use a "dirty" crucible so that if the initial guess is too high, it will not matter if the glass reacts and the crucible is ruined for precision measurements)

1. Prepare glass disks of the glass types that are being investigated. They should be small enough in diameter to fit inside the platinum pans for the DSC (approximately 5.75 mm in diameter is sufficient). These disks should have parallel surfaces so that one surface is polished and the other is fine-ground. Thickness should be approximately 1 mm.

2. Equilibrate the glass samples at a temperature, T_e, approximately 30°C below the annealing point temperature of the glass for approximately 120 hours depending upon glass composition.

3. Perform a test run on the glass sample in question in a platinum sample pan **not used for these precision measurements ("dirty" crucible)**. Perform this test run to try and determine an appropriate maximum temperature. The reason for using a different sample pan (perhaps a "dirty" sample pan that does not have a nice flat, undamaged bottom) is in the event that a maximum temperature chosen is too high and the glass sticks to the pan. At this point, the sample pan would have to be very carefully cleaned, and most likely not re-usable. A good first guess for this maximum temperature is approximately $125^{\circ}C$ above T_e of the glass samples

4. The DSC runs should be made with **platinum** reference and platinum sample pans. Note that the sample platinum pan used for the temperature calibration of the investigated glass type **should also be used for the following DSC runs**.

5. To perform the three DSC runs enter the TA Instruments software and ensure that you are in calibration mode. Run #1 should be made of a blank sample pan applying isothermal holds at $100^{\circ}C$ and the maximum temperature. Run#2 should be made of a sapphire sample (provided by the vendor), again, with isothermal holds at $100^{\circ}C$ and the maximum temperature – result is a matrix of $[T\ \Delta T_{st}]$. The sapphire samples used were 0.83 mm thick with a diameter of 4.75 mm and polished parallel surfaces – the result is a matrix of $[T\ \Delta T_{gl}]$. The mass was approximately 60 mg. Run #3 should be made of the glass sample in question with a 5 minute isothermal hold at $100^{\circ}C$ and the maximum temperature. The polished surface should be in direct contact with the bottom of the platinum pan.

With the appropriate dimensions mentioned in Step 1, the mass should be approximately 75 – 125 mg depending on glass type.

    a. Under the Summary Tab

        i. Select baseline for the sample name

        ii. The mass of the sapphire or glass should be recorded in the comments box and used for later calculations

        iii. Select location for the placement of the file

        iv. Select "custom" as the test procedure

    b. Under the Procedure Tab

        i. Make edits to the procedure by clicking "Edit"

        ii. Select "Ramp" and enter 10 K min^{-1} to 100°C

        iii. Select "Isothermal" and enter 5

        iv. Select "Ramp" and enter the investigated scanning rate to the maximum temperature

        v. Select "Isothermal" and enter 5

        vi. Select "OK"

6. Once the blank, sapphire, or glass sample is loaded into the DSC cell and the TA Instruments software is set up (Step 5) click "Apply" in the TA Instruments software window. Ensure that the procedure specified in 5.b is displayed on the right side of the screen directly above the "Heat Flow versus Temperature" graph. If all changes and adjustments made were applied by clicking the "Apply" button, the "play" symbol at the top left of the screen will be displayed green.

7. Click the green "play" symbol to start the method.

8. Follow the procedure spelled out in Step 5 – 6 for Run #1, 2, and 3.

9. Next, **all three runs** need to be corrected, or "rotated" with respect to their isothermal positions:

    a. Open the Universal Analysis software

    b. Open run #1

    c. In the "Data File Information" window ensure that Exotherm "Down" is selected

    d. Click on "Signals"

    e. Select "Delta T (mV/mg)" as "Y1"

    f. Select "Not used" as "Y2"

    g. Select "Time (min)" as "X"

    h. Click "OK"

    i. Click "OK"

    j. Since the user did not enter the mass in the correct space (mass was specified as "0.000 mg"), for the experiment, when following through with 8.h, a warning label will say "Cannot use normalized units with zero mass". This is OK as the mass will be data will be analyzed with the mass by the user manual at a future time. Click "OK".

    k. Once the file data is displayed in a window in the Universal Analysis software (Delta T / µV **versus** Time / min), click on "Tools"

    l. Select "Rotate"

m. The first point to indicate on the curve should be at the end of the first isothermal hold, and the second point should be at the end of the second isothermal hold. Once these points are adjusted by the user by placing the red placers in these positions:

    i. Right-click and select "Manual Limits"

    ii. For Point 1 X, enter the time (min) where the first isothermal hold ends. For Point 1 Y, enter 0.

    iii. For Point 2 X, enter the time (min) where the second isothermal ends. For Point 2 Y, enter 0.

    iv. Click "OK"

n. Right-click in the background of the data file

o. Go to "X-axis" and select "Temperature ($^{\circ}$C)"

10. Repeat step 9 for Run #2 and #3.

11. Once all three runs have been rotated, export each data file

a. Select "View from the Toolbar

b. Select "Data Table"

c. Enter the desired start temperature for exporting the data (The only requirement is that it is well below the transition region – 100°C is a good start temperature)

d. Enter the desired end temperature (maximum temperature of the measurement)

e. For temperature increment, enter 0.5°C

12. The subsequent data files should be saved as text files and exported for further use in Excel

13. Apply the Temperature correction determined from Appendix B to all three runs.

14. Subtract the data of Run #1 from both Run #2 and Run #3.

15. Compute the thermal resistance, R, between the furnace and the crucible

    a. Divide ΔT_{st} by the heating rate (K/s) and the mass (g) of the sapphire

    b. Plot ΔT_{st} normalized for the mass and heating rate versus T in Origin.

    c. Plot $c_{p,st}$ versus T in Origin

    d. Divide the ΔT_{st} by $c_{p,st}$.

    e. The result is R as a function of T.

    f. Import the R values back into excel.

16. Compute the temperature derivative of ΔT_{gl}

    a. Plot the corrected (temperature and baseline) [T ΔT_{gl}] in Origin.

    b. Use Origin to compute the derivative.

    c. The result is $\Delta \dot{T}_{gl}$ as a function of T.

    d. Import the $\Delta \dot{T}_{gl}$ values back into excel.

17. Now, all necessary values for the computation of c_p are in the excel file. Calculate the c_p of the glass sample from the following equation in excel as a function of Temperature according to the equation below

$$c_{p,gl} = -\frac{\Delta T_{gl} + \Delta \dot{T}_{gl} \cdot \dot{T} \cdot \tau_c}{R \cdot \dot{T} \cdot m} \tag{D.1}$$

REFERENCES

1.   Maschmeyer, R.O., et al., "Precision molded-glass optics," *Appl. Optics,* **22**[16] 2410-2412(1983).

2.   Mukasa, K., *Device and Method for Molding Optical Components*. 2003, Fuji Photo Optical Co., Ltd.

3.   Angle, M.A., G.E. Blair, and C.C. Maier, *Method for Molding Glass Lenses*. 1974, Eastman Kodak Company.

4.   Shelby, J.E., *Viscosity of Glass Forming Melts*, in *Introduction to Glass Science and Technology*. 2005, The Royal Society of Chemistry: Cambridge, UK. p. 111-137.

5.   Katsuki, M. *Transferability of Glass Lens Molding*. in *Advanced Optical Manufacturing Technologies*. 2006: Proc. of SPIE.

6.   Jain, A. and A.Y. Yi, "Numerical Modeling of Viscoelastic Stress Relaxation During Glass Lens Forming Process," *J. Am. Ceram. Soc.,* **88**[3] 530-535(2005).

7.   Jain, A. and A.Y. Yi, "Finite Element Modeling of Structural Relaxation During Annealing of a Precision-Molded Glass Lens," *J. Man. Sci. and Eng.,* **128** 683-690(2006).

8.   Yi, A.Y. and A. Jain, "Compression Molding of Aspherical Glass Lenses–A Combined Experimental and Numerical Analysis," *J. Am. Ceram. Soc.,* **88**[3] 579-586(2005).

9.   Klocke, F., et al., "Finite element analysis of glass moulding," *Proc. Instn Mech. Engrs, Part B: J. Engineering Manufacture,* **222** 101-106(2008).

10.   Scherer, G.W., *The Glass Transition*, in *Relaxation in Glass and Composites*. 1986, John Wiley & Sons: New York. p. 1-15.

11.   Tool, A.Q., "Relation Between Inelastic Deformability and Thermal Expansion of Glass in its Annealing Range," *J. Am. Ceram. Soc.,* **29**[9] 240-253(1946).

12.   Markovsky, A. and T.F. Soules, "An Efficient and Stable Algorithm for Calculating Fictive Temperatures," *J. Am. Ceram. Soc.,* **67** 56-57(1984).

13.   Sellier, M., et al., "An iterative algorithm for optimal mould design in high-precision compression moulding," *Proc. Instn Mech. Engrs, Part B: J. Engineering Manufacture,* **221** 22-33(2007).

14.   Fulcher, G.S., "Analysis of Recent Measurements of the Viscosity of Glasses," *J. Am. Ceram. Soc.,* **8** 339-355(1925).

15.   Angell, C.A., "Relaxation in liquids, polymers and plastic crystals - strong/fragile patterns and problems," *J. Non-Cryst. Solids,* **131-133** 13-31(1991).

16.   Bohmer, R., "Non-linearity and non-exponentiality of primary relaxations," *J. Non-Cryst. Solids,* **172-174** 628-634(1994).

17.   Wang, L.M., V. Velikov, and C.A. Angell, "Direct determination of kinetic fragility indices of glassforming liquids by differential scanning calorimetry: Kinetic versus thermodynamic fragilities," *J. Chem. Phys.,* **117**[22] 10184-10192(2002).

18.   "Standard Test Method for Annealing Point and Strain Point of Glass by Beam Bending," *ASTM,* **C 598-93** (2003).

19.   "Standard Test Method for Measurement of Viscosity of Glass Between Softening and Annealing Range (Approximately 10^8 Pa s to Approximately 10^{13} Pa s) by Beam Bending (Metric)," *ASTM,* **C 1350M-96** (2003).

20.   "Standard Test Method for Measurement of Viscosity of Glass Between 10^4 Pa s and 10^8 Pa s by Viscous Compression of a Solid Right Cylinder," *ASTM,* **C 1351M-96** (2002).

21.   Hagy, H.E., "Experimental Evaluation of Beam-Bending Method of Determining Glass Viscosities in the Range 10^8 to 10^{15} Poises," *J. Am. Ceram. Soc.,* **46**[2] 93-97(1963).

22.   Busch, R., E. Bakke, and W.L. Johnson, "Viscosity of the Supercooled Liquid and Relaxation at the Glass Transition of the $Zr_{46.75}Ti_{8.25}Ni_{10}Be_{27.5}$ Bulk Metallic Glass Forming Alloy," *Acta Mater.,* **46**[13] 4725-4732(1998).

23.   Fan, G.J., H.J. Fecht, and E.J. Lavernia, "Viscous flow of the $Pd_{43}Ni_{10}Cu_{27}P_{20}$ bulk metallic glass-forming liquid," *J. App. Phys.,* **84**[4] 487-489(2004).

24.   Glade, S.C. and W.L. Johnson, "Viscous flow of the $Cu_{47}Ti_{34}Zr_{11}Ni_8$ glass forming alloy," *J. App. Phys.,* **87**[10] 7249-7251(2000).

25.   Fontana, E.H., "A Versatile Parallel-Plate Viscometer for Glass Viscosity Measurements to 1000^oC," *Ceramic Bulletin,* **49**[6] 594-597(1970).

26. Dienes, G.J. and H.F. Klemm, "Theory and Application of the Parallel Plate Plastometer," *J. App. Phys.,* **17** 458-471(1946).

27. Gent, A.N., "Theory of the Parallel Plate Viscometer," *Brit. J. Appl. Phys.,* **11** 85-87(1960).

28. Schenk, C., *Viscosity of SCHOTT Glass Types.* 2007.

29. Malek, J., "Structural Relaxation of As_2S_3 Glass by Length Dilatometry," *J. Non-Cryst. Solids,* **235-237** 527-533(1998).

30. Malek, J. and J. Shanelova, "Structural Relaxation of As2Se3 Glass and Viscosity of Supercooled Liquid," *J. Non-Cryst. Solids,* **351** 3458-3467(2005).

31. Fotheringham, U., ed. *Analysis of the Composition and Structure of Glass and Glass Ceramics.* Schott Series on Glass and Glass Ceramics, ed. H. Bach and D. Krause. 1999, Springer-Verlag: Berlin, Germany. 338-344.

32. Fotheringham, U., et al., "Evaluation of the calorimetric glass transition of glasses and glass ceramics with respect to structural relaxation and dimensional stability," *Thermochim. Acta,* **461** 72-81(2007).

33. Gottsmann, J., D.B. Dingwell, and C. Gennaro, "Thermal Expansion of Silicate Liquids: Direct Determination Using Container-Based Dilatometry," *American Minerologist,* **84** 1176-1180(1999).

34. DeBolt, M.A., et al., "Analysis of Structural Relaxation in Glass Using Rate Heating Data," *J. Am. Ceram. Soc.,* **59**[1-2] 16-21(1976).

35. Fotheringham, U., ed. *Analysis of the Composition and Structure of Glass and Glass Ceramics.* Schott Series on Glass and Glass Ceramics, ed. H. Bach and D. Krause. 1999, Springer-Verlag: Berlin, Germany. 313-338.

36. Malek, J. and S. Montserrat, "Rate-determining factors for Structural Relaxation in Non-crystalline Materials II. Normalized Volume and Enthalpy Relaxation Rate," *Thermochim. Acta,* **313** 191-200(1998).

37. Moynihan, C.T., et al., "Dependence of the Fictive Temperature of Glass on Cooling Rate," *J. Am. Ceram. Soc.,* **59**[1-2] 12-16(1976).

38. Easteal, A.J., et al., "Heat Capacity and Structural Relaxation of Enthalpy in As_2Se_3," *J. Am. Ceram. Soc.,* **60**[3-4] 134-138(1977).

39. Narayanaswamy, O.S., "A Model of Structural Relaxation in Glass," *J. Am. Ceram. Soc.,* **54**[10] 491-498(1971).

40. Scherer, G.W., *Fictive Temperature*, in *Relaxation in Glass and Composites*. 1986, Wiley & Sons: New York. p. 113-129.

41. Kakiuchida, H., K. Saito, and A.J. Ikushima, "Fictive-temperature dependence of structural relaxation in silica glass," *J. App. Phys.,* **94**[3] 1705-1708(2003).

42. Hodge, I.M. and A.R. Berens, "Effects of Annealing and Prior History on Enthalpy Relaxation in Glassy Polymers. 2. Mathematical Modeling," *Macromolecules,* **15** 762-770(1982).

43. Hodge, I.M., "Enthalpy Relaxation and Recovery in Amorphous Materials," *J. Non-Cryst. Solids,* **169** 211-266(1994).

44. Fotheringham, U., et al., "Refractive Index Drop Observed After Precision Molding of Optical Elements: A Quantitative Understanding Based on the Tool–Narayanaswamy–Moynihan Model," *J. Am. Ceram. Soc.,* **91**[3] 780-783(2008).

45. Hodge, I.M., "Effects of Annealing and Prior History on Enthalpy Relaxation in Glassy Polymers. 6. Adams-Gibbs Formulation of Nonlinearity," *Macromolecules,* **20** 2897-2908(1987).

46. *Orton Model BBV-1000 Beam-Bending Viscometer*. 2003, Westerville, OH: Edward Orton Jr. Ceramics Foundation.

47. *Orton Model PPV-1000 Parallel-Plate Viscometer*. 2007, Westerville, OH: Edward Orton Jr. Ceramics Foundation.

48. "Optical Glass - Datasheets," *Schott Glass, Inc.* www.schott.com.

49. *Standard Reference Material 710a: Soda-Lime-Silica*. 1991, National Institute of Standards and Technology.

50. *TMA 2940 Thermomechanical Analyzer Operator's Manual*. 1993, New Castle, DE: TA Instruments.

51. *DSC 2920 Differential Scanning Calorimeter Operator's Manual*. 1998, New Castle, DE: TA Instruments.

52. "Standard Test Method for Determining Specific Heat Capacity by Differential Scanning Calorimetry," *ASTM,* **E 1269** (2005).

53. Hohn, G.W.H., W.F. Hemminger, and H.J. Flammersheim, *Theoretical Fundamentals of Differential Scanning Calorimeters*, in *Differential Scanning Calorimetry*. 2003, Springer: New York. p. 31-48.

54. Fotheringham, U., *Industrial Practice of Dilatometric Measurements*. 2008.

55.   Moynihan, C.T., et al., "Dependence of the Glass Transition Temperature on Heating and Cooling Rate," *J. Phys. Chem.,* **78**[26] 2673-2677(1974).

56.   Moynihan, C.T., et al., "Estimation of the Activation Energies for Structural Relaxation and Viscous Flow from DTA and DSC Experiments," *Thermochim. Acta,* **280/281** 153-162(1996).

57.   Fotheringham, U., ed. *The Properties of Optical Glass*. Schott Series on Glass and Glass Ceramics, ed. H. Bach and N. Neuroth. 1995, Springer-Verlag: Berlin, Germany. 203-230.

58.   Shelby, J.E., *Structure of Glasses*, in *Introduction to Glass Science and Technology*. 2005, The Royal Society of Chemistry: Cambridge, UK. p. 72-107.

59.   Hohn, G.W.H., W.F. Hemminger, and H.J. Flammersheim, *Types of Differential Scanning Calorimeters and Modes of Operation*, in *Differential Scanning Calorimetry*. 2003, Springer: New York. p. 9-13.